ENSO simulated by Intermediate Coupled Models and evaluated with observations over 1970-1996.

Part II: Sensitivity to the eastward penetration of the equatorial westerlies and to the off-equatorial ocean discharge-recharge associated with meridional winds.

by

C.Perigaud, C. Cassou, and F. Melin

submitted to Journal of Climate

July 14th, 1998

Jet Propulsion Laboratory, MS 300/323, 4800 Oak Grove Dr., Pasadena, CA 91109.

email=cp@pacific.jpl.nasa.gov

Abstract

Introducing new parameterizations of subsurface temperature and atmospheric convection in the Cane and Zebiak's model allows to reproduce oscillations with a period close to 4 years, equatorial wind anomalies that are located close to the dateline and realistic amplitudes of SST, wind and thermocline anomalies in the equatorial Pacific both in warm and cold phases. When the weight given to the atmospheric convection term is increased, the simulated wind maximum along the equator is displaced further west and the amplitude and duration of the warm events decrease. Compared to the simulations with the standard parameterization, the ENSO-like oscillations are not lost when the friction is increased with a decay time ranging from 30 to 12 months. Off-equatorial baroclinic ocean and wind anomalies are much less strong, but still necessary for the system to oscillate. Unrealistic easterlies are still present in the eastern off-equatorial Pacific and make the ocean loose heat content after the warm peaks. Unrealistic equatorial easterlies east of 80°W also make the coupled system easily loose its oscillatory behavior.

Replacing the atmospheric model by a statistical relationship between SST and wind stress anomalies allows to further reduce these deficiencies. The coupled model then simulates ENSO-like events in good agreement with observed oceanic and atmospheric fields in terms of amplitude and spatial patterns within 15° of the equator. Sensitivity tests to the statistics prescribed in the atmospheric component show that the model simulates warm events with duration and amplitude that increase with the eastern penetration of the westerlies in the Central Pacific, whereas stronger cold events do not last longer and easterlies remain located at the dateline. Depending on the strength of the warm event, the Southern ocean looses heat content or not after the peak of the event. Balancing the anticyclonic curl due to the northerlies along the ITCZ, the Northern ocean gets recharged with heat content after the warm peak. It re-fills the equatorial heat content prior to the growth of the following warm event. Some similarity can be found with the observed events.

1. Introduction

This second part is devoted to the understanding of Intermediate Coupled Models derived from the Cane and Zebiak's model (Zebiak and Cane, 1987) named CZ, where both the oceanic and the atmospheric components are modified according to the information given by observations. Results from Part I have shown that the use of the new subsurface temperature parameterization derived from hydrographic profiles does not allow to recover cold events when the ocean is coupled to the standard atmosphere. Neither does the introduction of a convection term derived from ISCCP data when the atmosphere is coupled to the standard ocean. The coupled simulations are all biased towards strong warm SST in the eastern Pacific, westerlies in the Central Pacific and upwelled thermocline in the western Pacific. In addition, they all present off-equatorial thermocline displacements and wind stress curl anomalies that are unrealistically large, mislocated, and play a key role in the oscillatory regime. Like in part I, "off-equator" means the southern and northern bands of latitude between 7° and 15°. The reader is invited to consult part I for abbreviations and conventions.

The CZ model is based on physics that have a reasonably good skill in reproducing the reality when it is run in a forced context. Skill is lost in a coupled context mostly because nonlinearities make coupled modes grow preferentially over the many different modes of variability simulated in a forced context. These coupled modes highly depend on the climatological background which feeds the asymmetry between warm and cold events because of its strong contrast between the East and the West, the North and the South. In this paper, the Tsub change in the mixed layer and the Conv change in the atmosphere are combined to form a new ICM named Tsub.Conv. Both changes suppress two important nonlinearities of the CZ model (see Part I). In Nature cold events are not the opposite of warm events either, they differ in timing, amplitude and location of the SST, thermocline and wind anomalies. Nonlinearity is still present in Tsub.Conv because of the climatology in the ocean mixed layer, in the transformation of wind into wind stress anomalies and in

the local heating of the atmosphere (see Appendix). Anomalous easterlies in the wind forcing of the ocean component tend to induce stronger oceanic response in SST Niño3 than anomalous westerlies of equal amplitude. Similarly when the atmosphere is forced by equally strong cold or warm SST anomalies, it develops zonal wind stress anomalies in the central Pacific that are more intense in easterlies than westerlies. Tsub.Conv privileges cold conditions in a forced context, it is wondered whether these tendencies balance out in a coupled context, i.e. the anomalies simulated by the model are neither biased nor drifting away twoards a warm or a cold state with time.

The first part of this second paper consists in analyzing the coupled regime simulated by the Tsub.Conv model. Its sensitivity to the weight given to the convection term in the atmosphere is examined in section 2. Its dependance on the off-equatorial signals as well as the impact of increasing the friction are presented in Section 3. In the rest of the paper, the atmospheric model is replaced by a statistical model named Astat that is described in Section 4. The coupled behavior of Tsub.Astat is examined in Section 5. The model sensitivity to the data used to build the statistical atmosphere is investigated in section 6. The mechanisms involving the off-equatorial variability are described in Section 7. Results and perspectives in terms of forecasting ENSO are discussed in the last section. Following the conventions adopted in Part I, the experiments presented hereafter are identified with a name for the model and a number in parenthesis for the run. Run identifications are listed in Table 1.

2. Coupled behavior of Tsub.Conv with a 30 month friction

In this section, the model is run with a friction decay time equal to 30 months like in CZ (run 1a). It is first run with the Tsub and Conv parameterizations derived from data in an experiment named Tsub.Conv (run 3a) and then with different weights for the atmospheric convection.

a) Oscillatory regime and variability patterns.

Tsub.Conv (run 3a) simulates oscillations with a period close to 4 years (Fig. 1). Like in CZ, oscillations present some irregularity and are phase locked with the seasonal cycle. The wind is reversing from easterly during cold event to westerly during warm event with a similar strength. The amplitude of SST Niño3 (Fig.1a), wind Niño4 (Fig. 1b) and thermocline Niño3 (Fig.1c) correspond to observations for mild to strong events; extrema are sligthly too small to represent very strong El Niños such as the 1982-1983 or the 1997-1998 events. The thermocline displacements over NiñoW (Fig. 1d) are larger than in reality for mild events (compare with Fig 1 in Part I), but upwelled positions are much more reasonable than the ones simulated by CZ, Tsub.CZ or CZ.Conv (compare with Fig. 3, 11, and 16 in Part I) and the averaged position over 30 years is close to normal. Conversely to CZ , there is no lag between the wind and the SST. There is no lag either between the SST and the thermocline in the east and all time series are very well correlated (more than 0.90). The thermocline downwellings in the western Pacific start simultaneously with the upwellings in the eastern Pacific and last a little longer. There is some assymetry with respect to warm/cold events duration, the former being longer than the latter. Note that although the friction is still weak, there is not much variability for frequencies higher than the year.

The SST variability (Fig. 2a) presents two maxima, one along the equator located at 135°W and one along the coast at 3°S-85°W. This agrees reasonably well with the observed variability, although the off-shore equatorial maximum is shifted to the west and has a slightly larger amplitude (compare with Fig. 2 in Part I). The wind anomaly patterns (Fig. 2b) are also in much better agreement with the observations than CZ or Tsub.CZ (compare with Fig. 4 and 12 in Part I). The maximum anomaly along the equator is located at 170°W, compared to 150°W with the standard atmosphere and 180° in reality. These maps resemble the variability simulated by CZ.Conv (compare with Fig. 13 in Part I) with some improvement in terms of amplitude. The wind anomalies are located slightly eastward of the latter. Tsub.Conv simulates a weak meridional wind component (Fig2c). It is weaker

than in CZ, but also than in reality along the ITCZ or the SPCZ. The amplitude of the thermocline variability (Fig. 2d) is considerably reduced, it is now weaker than in reality in the central equatorial Pacific and it is still overestimated in the eastern and western Pacific North of 5°N .

b) Sensitivity to the atmospheric convection

As explained in Part I, the Conv atmosphere is driven by a local heating term Q_T and a convective heating term Q_{CN}. The amplitude of each term is determined by the parameters α and γ, which are respectively equal to 0.015 $m^2\ s^{-3}\ °C^{-1}$ and 1.13 x 10^4 $m^2\ s^{-2}\ °C$. The latter was determined by best fitting the cloud convection and the SST observations over the 1983-1991 period when both data sets were available. Its value actually depends on the period of the fit (see DP96). The sensitivity of Tsub.Conv to the strength of the convective heating relative to the local heating is tested by running coupled experiments where the ratio γ / α is changed to values ranging from 0 to 2. The case "ratio = 1" corresponds to Tsub.Conv (run 3a). The case "ratio = 0" corresponds to the atmosphere driven by local heating only like in Gill (1980) and is named Tsub.Gill.

Simulated SST and wind patterns are sensitive to this ratio (Fig. 3). Similarly to the forced context, increasing the relative weight of convective forcing allows to drag the wind westward. However in a coupled context, it also significantly affects the amplitude and the timing of the events (see Table 2). Tsub.Gill simulates the wind at the easternmost location and has the strongest amplitude and the longest duration of warm events. Indeed its anomalies have a mean bias towards warm states similar to CZ.Conv (run 4). Its wind and SST maxima are nevertheless located westward of CZ.Conv (compare Fig 3ab with Fig. 15ab in Part I) because the Tsub change also contributes to drag the coupled patterns westward. If the convective term is weaker than in run 3a (Tsub.Conv run3b), the wind is still to the East of reality, the amplitude of the oscillations are still larger and the period is close to 4 years. If the convective term is stronger (run3c), the wind maximum is located close to observations, but the amplitude of the coupled oscillations get much weaker and

the period much shorter. Thus the amplitude and duration of the warm events increase with the eastern penetration of the westerlies. Interestingly, cold events are not as much affected. The negative SST anomalies never last longer than in run 3a. In addition, note that all experiments simulate a large wind variability east of 100°W which corresponds to strong easterlies during warm events. Like in CZ, these are responsible for the sharp decrease of SST amplitude towards the American coast in run 3b or Tsub.Gill (Fig. 3a). All these features correspond to mechanisms involved in the coupling between the baroclinic ocean, the ocean mixed layer and the atmosphere that are described below by examining the various terms of the T equation simulated by Tsub.Conv (run 3a).

Like in Part I (Fig. 7), budgets are presented along the equator in the western, central and eastern Pacific for the horizontal advection, the two vertical mixing terms and the local rate of change corrected by the damping (Fig. 4). The mechanisms simulated in Tsub.Conv (run 3a) are very different from the ones simulated in CZ. In the eastern Pacific, the thermocline displacements in term T6 are responsible for a large part of the SST tendencies (Fig4c). As found in observations, the subsurface temperature anomaly due to thermocline displacements in the East is larger than the surface anomaly. So an upwelled thermocline cools down the SST and a downwelled thermocline warms it up. This corresponds a lot more to our understanding of what happens in reality or what happens in simulations forced by observed winds (see DP96). Note that the anomalous upwelling rate (term T5) is not contributing much to the SST variations. On average between 120°W and 80°W, the westerlies and the meridional wind convergence are hardly strong enough to cancel out the upwelling due to the easterlies blowing east of 100°W. The latter induce a local anomalous upwelling which has a negative coupled feedback on the system like in CZ. Even though the easterlies are weaker than in CZ, the meridional wind anomalies are also weaker, they have a weak convergence and they are located in the central Pacific eastward of CZ. Thus they are not efficient in compensating the negative feedback of the

spurious zonal wind anomalies East of 100°W and Tsub.Conv can easily loose its oscillatory behavior.

In the central Pacific (Fig4b), the behavior is similar to CZ with respect to term T5 sustaining the SST trends and term T6 competing them. However Tsub.Conv simulates a cooling impact in case of upwelled thermocline of the same strength as the heating impact in case of downwelled thermocline. Interestingly, the heating due to term T6 leads the SST warming trends by a few months.

In the western Pacific (Fig4a), changes are due to the baroclinic modes (term T1 and term T6) which are dominant during cold events. Easterlies induce strong baroclinic current anomalies that move the cold waters from East towards the warm pool. Downwelled thermoclines have a stronger impact than upwelled thermoclines. So term T6 is very efficient to terminate cold events that do not last as long as warm events. Actually the heating impact of the downwelled thermocline overshoots the erosion of the cold events and kicks in the following warm event. After the recovery of the cold event, term T6 indeed triggers the warming trends in the West before the eastern Pacific starts warming.

Budgets were analyzed with the model outputs for run 3b and 3c. Changing the weight of the atmospheric convection does not affect much these budgets during cold events, whereas it does during warm events. For run 3b, because the coupled system has stronger warm events with westerlies along the equator located more eastward and curl anomalies located more poleward, term T5 grows and extends more eastward once the kick-in of a warm event by term T6 has taken place in the western Pacific. Term T6 associated with the upwelled thermocline in the western off-equatorial basin also grows and penetrates equatorward and eastward to erode the growing warm events. These last longer then because it takes more time for the upwelled ocean to propagate to the western boundary and reflect in the equator to reverse the warming trend of the central and eastern Pacific. Similarly the mass adjustment via the interior takes more time as the Rayleigh coefficient is not changed and the mass sinks are further away from the equator. For run

3c, the coupled anomalies are more confined to the equator and negative heat content anomalies are available sooner to erode the growth of warm events and reverse them.

Without changing the amplitude of the Conv parameterization which has been derived by best fitting data, the Tsub.Conv model (run 3a) reproduces the westernmost location of the wind for a reasonable amplitude of events. Trying to further drive the wind to the West of 170° by increasing the strength of the atmospheric convection is not successful because of the drastic drop of amplitude. Increasing the drag coefficient by 20% in an experiment with the ratio of run 3c (not shown) allows to recover a realistic amplitude, but it locates the wind back in the Central Eastern Pacific as in run 3b. Let us examine if increasing the dynamic friction reduces the deficiencies mentioned above, namely the overly large zonal wind anomalies and thermocline displacements in the off-equatorial Pacific.

3. Sensitivity of Tsub.Conv to the dynamic friction

Results from Part I illustrate that coupled simulations are extremely sensitive to friction, especially since the off-equatorial ocean and wind variations are involved in the coupled behavior. For example, the CZ model simulates oscillations that do not resemble ENSO any more with a friction decay time shorter than 30 months.

Tsub.Conv is now run with a decay time equal to 6 months instead of 30 months in an experiment named (run 4). The indices oscillate with weak amplitudes and a period close to 1.3 year (Fig. 5a). Increasing the coupling coefficient by 20% (run 5) leads to oscillations around a warm permanent state. Tests (not shown) with various initial conditions or coupling coefficients reproduce different regimes, but none has an ENSO-like behavior. It is tempting to say that the equatorial ocean with one vertical mode and realistic parameters is not able to maintain an ENSO-like regime when coupled to the Conv atmosphere. But despite the many tests which all fail to reproduce realistic oscillations, such general statements should be avoided. Coupled simulations are model dependent.

Indeed, Battisti (1988)'s model which also assumes a 30-month Rayleigh friction, does not need the off-equatorial wind variability to oscillate and may keep its oscillatory regime with a 6-month friction.

With frictions stronger than (12 month)$^{-1}$, the model does not have an ENSO-like behavior although various coupling coefficients were tested. With a friction coefficient equal to (15 month)$^{-1}$ or (12 month)$^{-1}$ and with the same initial conditions and coupling coefficient as in run 3a, Tsub.Conv still has an unrealistic behavior like in run 4. Increasing the coupling coefficient by 20% allows the model with a friction of 15 months (run 6) or 12 month (run 7a) to simulate interannual events that have reasonable amplitudes and periods (Fig. 5bc). Both runs have similar amplitudes, but the Niño3 index is misleading. Off-equator the amplitude and patterns of the events are very different. Run (6) has much larger amplitudes of thermocline displacements (Fig. 6a) and wind stress curl anomalies (Fig. 6b) than (run 7a) which is similar to (run 3a). Its thermocline displacements in the western Pacific are as large as in CZ. Runs 3a and 7a have an amplitude similar to observations in the South. It is still stronger in the North. The wind stress curl anomalies agree very well with observations along 9°S (not shown), but not along 9°N (Fig. 6b). The model overestimates the wind in the Central Northern Pacific and underestimates it west of the dateline and east of 120°W.

A series of experiments are performed like in Part I to examine if the model behavior depends on equatorial processes only or not. Run 7a which off-equatorial variability is much weaker than CZ or (run 6) is chosen as a reference for various filtering tests. The experiment (run 7b) where the off-equatorial wind is filtered out like in Battisti (1989) does not simulate oscillations, but stays in a permanent warm state (Fig. 5c). Tsub.Conv also needs the off-equatorial wind anomalies to oscillate. Interestingly, filtering out the reflection of Rossby modes higher than 5 at the eastern boundary (run7e) perturbs the oscillation, but does not make the model loose its oscillatory behavior (Fig. 5d). It does in the experiment where they are filtered out at the western boundary (run 7w).

Without the off-equatorial winds (run 7b) or the reflection of the off-equatorial ocean at the western boundary (run 7w), the model is not able to fully reverse the first warm event, it does not have enough source of cold from the western Pacific to terminate the event and it stays in a warm state. Without the reflection at the eastern boundary (run 7e), the first reversal is accomplished, but the subsequent oscillations are affected because the global mass adjustment is different. The fact that the off-equatorial thermocline displacements in the East are not necessary to sustain the oscillatory regime indicates that the off-equatorial ocean is much less drastically involved in the oscillatory regime than for CZ. Interestingly filtering out the eastern boundary in a Tsub.Conv experiment with a friction equal to 30 month (not shown) does suppress the oscillatory behavior again. So one must be careful in concluding about the role of the eastern boundary in ENSO. The scenario proposed by Picaut et al (1996) can be successfully reproduced by a coupled model or not, depending on the values chosen for the friction coefficient. Nevertheless like in CZ (See Part I), the off-equator does not contribute to the equatorial oscillations via reflection at the boundaries only. Similar filtering tests started from different initial conditions (not shown) simulate an index which stays quasi-normal for the 30 years, the model then lacks the off-equator to trigger growing events. Thus the off-equator plays a role via mass adjustment and transport in the interior of the domain as well. The mass transport simulated by run 7a across 5°S or 5°N (not shown) shows that the ocean (equator, North and South) looses heat content after the warm peak and prior to the next warming event, the equatorial ocean gets recharged by the off-equator. The recharge is slightly stronger from the North than from the South. Except for this assymetry and for the amplitude which is much weaker for Tsub.Conv than for CZ, these characteristics of ocean discharge-recharge resemble a lot the ones described in Part I section 5. We come back on this issue in Part II Section 7.

The spatio-temporal evolution simulated by Tsub.Conv (run 7a) is now described for one cycle of oscillations, with the time origin chosen at the second maximum of the double-peak warm event simulated by run 7a on year 9 (Fig. 7). The anomalies are quite

different from CZ (compare with Fig. 9 in Part I). There is very little energy at frequencies higher than the year. Although the model recovers faster from cold than from warm events, both phases evolve slowly. The thermocline front slowly propagates at 10cm/s to the east along the equator (Fig. 7d). Similar propagation is found for the zonal wind along the equator (Fig7e) or the thermocline in the eastern Pacific along 9°S (Fig. 7g). Westward propagation is found along 9°N and 9°S in the western Pacific where the wind stress curl is very weak (Fig. 7ag). Because of the coupling with the wind, the propagation speed (25 cm/s) is slower than the theoretical Rossby wave speed (32cm/s, dashed line in Fig7a) and consistent with the speed of coupled Rossby waves in the tropics (White et all, 1998). The SST is weaker in the North (Fig. 7c) than in the South. At the equator and South of it (Fig. 7fi) it presents two distinct features with the off-shore and coastal signals. The signal is maximum at the coast 4 months prior to the off-shore peak and peaks again 4 months after.

Hovmoeller diagrams are now compared with observations. Because data show that localisation, propagation, and timing of the anomaly maxima differ for each event, it is chosen to present a specific event rather than a composite one. The period presented in (Fig. 8) covers 1982-1985 with the origin of time at the January 1983 warm peak. Tsub.Conv simulates processes that correspond reasonably well to the 1982-1983 El Niño. In particular, slow eastward propagation of wind and thermocline anomalies along the equator is also observed (Fig. 8de). Thermocline anomalies propagate slightly faster than the wind (15 cm/s and 10 cm/s respectively). This mode of propagation resembles the slow mode proposed by Chao and Philander (1991) and reproduced in the forced context (see DP96). Slow eastward propagation is also found outside the equator in the SST along 5°N and the thermocline along 9°S (Fig8cg). The latter is quite remarkable indeed. Zonal wind anomalies during warm events resemble the simulated ones in amplitude and location as well as the wind stress curl along 9°S during the warm peak (Fig. 8h). However, the model misses wind energy in the western Pacific especially after the warm event. It is

striking that the simulated amplitude of the westerlies in the central Pacific along the equator corresponds to the one observed during a strong event, whereas the amplitude of the SST is weaker. This is due to the easterlies east of 80°W simulated by the model. The timing of the equatorial signals also differs from reality. Observed thermocline and westerlies are leading by about 4 months the off-shore SST maximum which leads the coastal warm peak by another 6 months. This sequence is nevertheless not systematically found for all observed events. It is not observed in the cold 1984-1985 period whereas it is systematically reproduced by Tsub.Conv. In the North, the agreement is not good for wind and thermocline. The model overestimates the low-frequency large-scale signal of the wind curl in the central Pacific and misses the signals in the west. Following the 1983 warm peak, the downwelled thermocline propagates all across the basin at about 45 cm/s faster than the theoretical free Rossby wave at that latitude (Fig. 8a). Thus the observed ocean is recharged with heat content all across the basin during that year whereas the simulated zonal averaged anomaly of heat content is actually negative. The fact that the simulated coupled regime highly depends on the off-equator and is highly sensitive to the choices of the friction and coupling coefficients is a major concern.

In summary, Tsub. Conv is able to reproduce interannual oscillations of SST, wind and thermocline which agree much better with observations than CZ in terms of location and strength of the anomalies. Cold events are reproduced without inter-event fluctuations. Thermocline upwellings in the eastern Pacific cool the system down whereas they happen to heat it up in CZ. The westerlies and the wind curl maxima are located 20° to 40° to the West of CZ. However like CZ, Tsub.Conv still simulates unrealistic easterlies East of 100°W along the equator that have a negative feedback. It simulates very weak meridional wind anomalies and strong easterlies in the off-equatorial Pacific during warm events that are not observed. The latter correspond to a pair of cyclonic curls on both sides of the equator and upwelled ocean on average zonally during at least one year past the warm event. Slight changes in the weight of atmospheric

convection, dynamic friction or coupling coefficient easily suppress the oscillatory behavior or drastically affects the balance between the equatorial and off-equatorial mechanisms at work to sustain the oscillations. This unrealistic horse-shoe pattern of easterlies in the eastern Pacific is typical of a Gill (1980)'s atmospheric response to the equatorial warm SST anomalies that are maxima off-shore. The weakness of the meridional wind anomalies in comparison with the observed ones along the ITCZ and SPCZ is another deficiency which can be attributed to the Gill's type of model. In order to examine if better could be done without these features, the Conv model is replaced by a statistical atmosphere in the following sections.

4. The Statistical Atmosphere

The statistical model is based on a Singular Value Decomposition between the SST and the wind stress anomalies which consists in capturing the coupled modes of variability as explained in Syu et al (1995). The two FSU wind stress components and the CAC SST data estimated on the CZ coarse model grid (5.625° x 2°) are decomposed over the Pacific between 19°S and 19°N over 15 years from January 1980 to December 1994. Similarly to the results of Syu et al (1995), the first seven modes explain 98.4% of the covariance between the SST and the winds, with 86.5% for the first mode, 8.4% for the second mode, 1.2% for the third and less than 1% for the higher modes. The first mode explains 38.6% of the SST variance over the domain, 17.8% for the zonal stress and 22.8% for the meridional component, the second mode 9.7%, 11.9% and 9.7% respectively, and the third mode less than 5% for all signals. Most of the unexplained variance is outside the equatorial band.

The eigenvalues of the first SVD SST and wind mode are very well correlated (Fig. 9a). Consistently with what is described in Part I, time series are better correlated by introducing a 1 month lead for the wind. Eigenvectors correspond to a warm anomaly with an offshore SST maximum at 150°W (Fig. 10a), westerlies centered around 170°W

(Fig10b), northerlies along the ITCZ and southerlies along the SPCZ (Fig. 10c). The second SVD mode corresponds to the coastal SST maximum (Fig. 10d), wind anomalies of the same sign to the East of mode 1 and of opposite sign to the West (Fig. 10e) and southerlies in the Southeast and northerlies everywhere else (Fig. 10f). The time series of this mode (Fig9b) are maxima during the second half of year 1983, corresponding to the full development of the strong event when the second warm peak is confined to the eastern boundary as seen in Fig. 8cfi. It is also strong in 1989, corresponding to the full development of the cold event with the easterlies extending unusually far West in the Pacific. In the 1990–s, the second mode is very weak. The sum of the first seven modes reproduces very well the observed signal. It gives a Niño3 SST index which agrees within 0.3°C rms with the observed one (Fig. 9c). Warm peaks are too weak though by a factor 1.4. The 7 modes sum up in a Niño4 TX index which agrees within less than 0.1 dyn/cm^2 rms with the observed one (Fig9d). The amplitude of the wind peaks is well recovered.

The statistical atmospheric model Astat consists in projecting the SST field at a given time on the 7 normalized SST eigenvectors to get the amplitude of each mode at that time which is then multiplied by the ratio between the wind and the SST normalization factor to provide the amplitude of the corresponding wind mode. The wind field at that time is then reconstructed by adding the contribution of the 7 wind modes. The normalization factors for each SST and wind mode are prescribed in the Astat model to the value that has been derived from the amount of observed variance explained by each mode over the decomposition period. It is thus assumed perfect correlation in time and perfect match in amplitude between the SST and the wind time series for each mode. Let us examine with the observations to what extent these assumpations are valid. The correlation between the SST and the wind time series is quite high for the first two modes (Fig9ab). It decreases with modes higher than 2 but this is not a major problem as long as the variance explained by these modes remains very small. More importantly, the Astat model neglects the slight phase shift between the wind and the SST for the first two modes, which precludes the

possibility of simulating wind anomalies with a leadtime relative to SST. In addition, the amplitude of SST mode 1 is slightly weaker than the amplitude of the corresponding wind mode, whereas it is the inverse for mode 2. One can expect that coupled simulations are sensitive to the values of the normalization coefficients. These details have important consequences examined in section 6.

Nevertheless, the Astat model forced by the CAC data reproduces the observed wind anomalies very well. Their Niño4 average agrees within 0.2 dyn/cm2 rms with the observed one (Fig. 9d). Except for the 1990_s, it misses some amplitude. Multiplying the SVD by a factor 1.4 allows to recover the amplitude of the warm peaks, but it gives a wind which is too strong. The coefficient that minimizes the sum of the misfit between the simulated and observed Niño3 SST index and Niño4 TX index is 1.2. Using this coefficient, the variability of the SST and wind anomalies simulated by Astat is presented in Fig.11 and can be compared with Figure 2 of Part I. Astat reproduces both SST off-shore and coastal maxima, the amplitude is however slightly weak. It reproduces the wind maximum at the dateline along the equator with the correct amplitude. The variability of the zonal wind is weaker beyond 5° of latitude, and along the equator east of 120°W and west of 150°E. It is found that the missing signal has a higher frequency than ENSO. Astat also misses some amplitude for the meridional wind component in the Southwestern Pacific, whereas it overestimates its variability along 5°N. Choosing a weaker coefficient than 1.2 would reduce this deficiency, but it would give weaker SST and zonal wind anomalies along the equator. As the equatorial processes are very important, we choose the value 1.2 as the reference drag coefficient in the Tsub.Astat forced experiments.

5. Coupled behavior of Tsub.Astat

a) Role of the friction and coupling coefficient

Tsub.Astat is first run with a friction coefficient equal to (6 month)$^{-1}$. Various coupling coefficients were tested but none gives an oscillatory regime as seen in Fig. 12a.

With the coefficient of reference (run 8), anomalies are damped to the normal state in less than 5 years and with a coefficient increased by 20% (run 9), anomalies stay warmer than 1°C. Depending on initial conditions, the model can end up in a permanent warm or cold state (not shown). Oscillations with a period ranging from 3 to 5 years are obtained when the friction is slightly decreased. Whether the friction coefficient is equal to $(12 \text{ month})^{-1}$ (Fig. 12b) or $(9 \text{ month})^{-1}$ (Fig.12c), the anomalies of the Niño3 index correspond to mild events. Experiments performed with increased coupling coefficient do not give stronger events. Whether the coupling coefficient is increased by 20% (run 11a) or not (run 10), Tsub.Astat reproduces similar amplitude (Fig. 12b). Increasing the coefficient only lengthens the period (40 months for run 10 and 57 months for run 11a). For a given coupling coefficient, changing the friction does not affect much the amplitude either, it rather affects the duration of the warm events too. Tsub.Astat reproduces warm events every 45 months with a friction of $(9 \text{ month})^{-1}$ (run 12a) instead of 40 months with a friction of $(12 \text{ month})^{-1}$ (run 10). The stronger the friction or the coupling coefficient, the longer it takes to recover from warm peaks.

Filtering out the off-equatorial wind similarly to Tsub.Conv in section 3 is tested with a friction of 12 (run 11b, Fig. 12b) or 9 month (run 12b, Fig. 12c) . Whatever the friction or the coupling coefficient, the filter does not suppress the oscillatory behavior. It does not affect much the amplitude either. It rather decreases the period as it speeds up the decay of warm events: peaks are simulated every 3 years for run 11b and every 30 months for run 12b. These experiments indicate that Tsub.Astat is a lot less sensitive to the off-equatorial variability than Tsub.Conv. In addition, the experiment (12w) where the high Rossby modes are filtered out before reflection at the western boundary also simulates ENSO-like oscillations (Fig 12d). Warm events come back then with a period close to 3 years which is slightly shorter than run 12a. It is plausible that the off-equatorial filters shorten the period of oscillations (run 11b and 12b compared to 11a and 12a), because the thermocline anomalies at the equator in the western Pacific are then fed only by the gravest

growing anomaly in the Central Pacific. Similarly for a given wind in the central Pacific, weakening the friction (run 10 compared to run 12a) allows to let the thermocline anomalies reach the western boundary with more amplitude and be more effective to reverse the SST tendencies sooner, therefore the period of oscillation is shorter. However this interpretation is dangerous because the off-equator does not only interact with the equator via reflection at the boundary. Indeed the experiment (12i) where the high Rossby modes are filtered out over the whole ocean model domain is successfully performed for Tsub.Astat (Fig12d). Conversely to CZ, the contribution of the mass adjusment in the interior domain involved by the high Rossby modes in the equatorial band does not violate the stability criterium (see Part I, section 5). Run (12i) simulates a first warm event that does not grow as efficiently as in the other filtering cases and the regime of oscillations during the whole 30 years is significantly different. Nevertheless Tsub.Astat is the model which is the least sensitive of all to the off-equatorial variability.

Whatever the friction, the coupling coefficient or the off-equatorial filter applied in Tsub.Astat, the model shows a robust oscillatory behavior. The amplitude of the variability for the SST or the zonal wind stress along the equator is not affected (Fig. 13ac). This is even the case off-equator for the wind stress curl or the thermocline anomalies (Fig. 13bd). This is a big difference compared to Tsub.Conv behavior. Signals are found very similar to the ones simulated in a forced context (named Tsub.Astat (0) in Fig. 13). The model data misfit can be partly explained by the SVD itself which misses some observed variability. This aspect is reinforced by the fact that the coupled model selects the first SVD mode of covariance even more drastically than in data. There is less percentage of variability explained by the SVD modes higher than the first one in experiment 12a than in the data decomposition. Whereas all modes have a normalized amplitude that has been determined to fit the data, mode 2 is counting for less than 1 (30%) relative to mode 1 and higher modes are even weaker. Interestingly, retaining the first mode only in Astat instead of the 7 as above, makes the model loose its oscillatory behavior. Adding the second mode

allows to recover oscillations that are very similar to experiments 10 to 12 and higher modes are not necessary to sustain the oscillations.

b) description of the variability patterns and oscillatory behavior

As soon as 2 SVD modes are retained, oscillations ressemble a lot the ones simulated by run 12a whatever the friction or the coupling coefficient. SST wind and thermocline variability have realistic patterns (Compare with Fig. 2 in Part I). The SST variability (Fig. 14a) presents an off-shore and a coastal maximum. Both the zonal wind (Fig. 14b) and the meridional wind (Fig. 14c) are in good agreement with the maps reconstructed from CAC observations. Compared to CZ or Tsub.Conv (Check Fig. 4 in Part I and Fig. 2 Part II), Tsub.Astat gives the most realistic wind, with the zonal wind maximum at the dateline and no anomalous patterns in the eastern Pacific (see also Fig. 13c). The two wind components ressemble a lot the ones reconstructed after the SVD (see Fig. 11), with the meridional wind in the North actually stronger than in the original wind data set. The wind thus converges with a maximum at 1°N and this explains why the SST off-shore maximum is located north instead of south of the equator. Finally although Tsub.Astat does miss some thermocline variability in the central Pacific, the amplitudes of the displacements in the eastern equatorial Pacific, in the Northwestern and Southwestern Pacific are now close to Nature (Fig. 14d).

Hovmoeller diagrams are presented for Tsub.Astat (run 12a) in Figure 15 and for observations during the mild 1986-1987 warm event in Figure 16. By contrast with Tsub.Conv (Fig.7) and the 1983 event (Fig. 8), slow eastward propagation is not detectable here. Along the equator, warm and cold anomalies in SST and wind agree reasonably well with observations. However the cold event does not last as long for the model. Tsub.Astat misses the lead of the wind relative to the SST signal and simulates a see-saw pattern for the thermocline that is not found in observations. The coastal SST peaks first iin the South and equator, the offshore signal continues to grow and peaks about 4 months later on both sides of the equator. Similar scenario is observed, including during

the cold event. Off-equatorial wind stress curl changes have similar amplitudes and signs for model and observation in the South. The simulated curl and the downwelled thermocline anomalies in the western Pacific are missing strength though in amplitude and duration during the cold event in the North.

The temporal evolution of the SST equation terms simulated in experiment 12a are presented in Figure 17 (left panels). As for Tsub.Conv, one of the major improvements compared to CZ is found in the eastern Pacific where a downwelled thermocline induces a warming and an upwelled thermocline a cooling (term T6, Fig17c1). Term T6 takes the leading role there and explains most of the SST tendencies. In the central Pacific (Fig. 17b1), term T5 dominates the other terms, most of it is due to the convergence of the meridional wind and is now confined there. Term T6 does not play an important role during warm events whereas its contribution to trigger the warming is crucial. It leads the SST trends by a few months. This feature is obvious in the western Pacific where at the begining of the warming trend, the thermocline is at its most downwelled position. Whereas no significant warming has occured in the East yet, it is already initiated in the West. Horizontal advection (term T1) plays an important role in this region too. During cold events, it has a positive feedback and brings climatological cold water from the central to the western Pacific. Compared to Tsub.Conv, term T5 plays a greater role over the western Pacific. In the eastern Pacific (fig17c1), it is weak but it always has a positive feedback. The growth of warm events is not threatened as in Tsub.Conv by spurious wind anomalies east of 80°W. Among the horizontal advection terms, T3 which benefits from the climatological heat source with the cold tongue extension in the South contributes to heat the system during the onset of the warm event.

Because the Tsub.Astat simulations forced by observed SST reproduce very well the various events observed over 1980-1995 and because the coupled behavior depends so much on the anomalous upwelling rate (T5) which is so hard to validate with data, it is worth comparing these results with the forced experiment. In the western Pacific (Fig.

17a2), the largest anomalies are found in 1984 and 1988 and correspond to the heating due to downwelled thermocline (term T6) and the cooling due to westward current anomaly (term T1) that are driven by the easterlies. This competition is similar to the behavior simulated in the coupled runs for Tsub.Astat and Tsub.Conv as well. For both models, cold events have a stronger signature in the western Pacific than the warm ones. In the Eastern Pacific (Fig. 17c2), term T6 explains a lot of the SST changes. It explains the warming prior to 1983, 1987 and 1992 events, it contributes to remove heat at the end of the 1983 warm event and to cool down during the cold event in 1988. This is in agreement to some extent with the coupled results. In case of particularly strong warm events like in 1983, term T6 warming trend is overpowered by the warming trend due to the locally induced downwelling (term T5). The latter explains the second warm peak observed in mid-1983. This is not reproduced in the mild events simulated by Tsub.Astat (12a). The central Pacific (Fig. 17b2) is the region where the forced simulations differ the most with the coupled ones. For example as soon as early 1983, the thermocline is responsible for a cooling term which is very strong and active during all the year to reverse the warm tendency due to the other terms. In 1983 after the first warm peak, the advection of anomalously warm waters from the East by the SEC (term T2) is responsible for a strong heating term that can be tracked all the way to the western Pacific. A strong cooling trend due to westward baroclinic current anomaly (term T1) is found in 1988. None of this is reproduced in the Tsub.Astat (12a) which privileges mild events like the 1986-1987 warm or 1984-1985 cold periods. Results may be different if the statistical atmosphere better represents the strongest events.

6. Sensitivity of Tsub.Astat to the statistical atmosphere.

To examine the sensitivity of the SVD approach to data errors or to the period over which the statistics are computed, different combinations of data sets have been decomposed such as the detrended FSU and the CAC series over 25 years between 1970

and 1994, the non-detrended FSU and the CAC series over the same period, or the detrended FSU and the Reynolds SST over the 15 years between 1980 and 1994. The SVD results are very robust. This is particularly true for the first two modes that explain more than 92% of the covariance between the wind and the SST. The first mode always explains about 40% of the SST and 15% of the zonal wind variance, the second mode about 20% and 10% respectively. Eigenvectors have similar patterns, with mode 1 associated to the off-shore SST maximum and wind maximum at the dateline and mode 2 associated to the coastal SST maximum and wind maximum in the eastern central Pacific. Furthermore eigenvectors, normalizations and time series obtained by these new decompositions are very similar to those described in section 4. Their differences are consistent with what is reported about the various data sets and events observed over 1970-1995 in Part I. For instance, the first eigenvector of the SST derived from Reynolds data has a signal more confined to the equator and the ratio between the first and second mode for SST is weaker by 5% than with CAC. The second SVD eigenvector of the wind is the one which is the most affected by the choice of the data set. Derived from the decomposition with the non-detrended FSU wind, it presents a pattern in the western Pacific which has a similar amplitude and the same sign as the pattern East of 140°W.

In addition, normalization coefficients depend on the strength of the events covered by the period of decomposition of course. Keeping in mind forecasting issues (manuscript in preparation), the FSU detrended winds and the CAC SST are also decomposed over 10 years starting 1970 to exclude data over the forecast 1980-1997 period. The ratio of the normalization of the second mode over the first one is then smaller, because the strongest peak of mode 2 over 1970-1980 occurs in 1977, when its strength is much weaker than in 1983. Nevertheless, these differences have a small impact on the ability of the Astat model to reproduce the observations. For example, the SST and the winds simulated over the period 1970-1980 with the SVD modes obtained over the period 1980-1995 agree well with the observed ones (Fig. 18ab). Similar conclusion can be drawn for the SST and the

winds simulated over the period 1980-1995 with the SVD modes obtained by the decomposition over the period 1970-1980 (Fig. 18cd). One can conclude that the statistical atmosphere model is skillful to simulate ENSO signals in a forced context, no matter which period and data sets are used to compute the eigenvectors and their normalizations. Aware that conclusions in a forced and a coupled context can be very different, the various SVD combinations are used below to test the sensitivity of the coupled model.

Indeed Tsub.Astat is found extremely sensitive to the SVD. Astonishingly, the model with the friction and coupling coefficients that have been used in Section 5 can loose its oscillatory behavior. This is the case in particular for the SVD derived from the non-detrended FSU because of the wind pattern in the western Pacific contained in the second eigenvector (this SVD precludes the reversal of the warming trends), and for the SVD derived from the Reynolds SST data because of the confinement of the SST first mode in the equatorial band (this SVD looses the positive feedback of term T3 during the onset of the warming). Replacing these eigenvectors by the ones derived from the detrended winds and from the CAC SST data allows to recover the oscillatory behavior. For the other combinations, oscillatory behavior is recovered by amplifying the normalization ratio of the second mode. This amplification strengthens the wind anomalies between 100°W and 140°W, in particular the westerlies along the equator the northerlies in the North and the southerlies in the South which have a positive feedback on the coupled system. Indeed all data decompositions show that the second wind mode has an amplitude slightly weaker than the second SST mode and this weakness prevents instabilities from growing in a coupled context.

Sensitivity tests are carried out to examine how the oscillatory regime is affected by changing the normalization ratios. Tsub.Astat is most sensitive to the ratio of the second mode. Slight changes lead to very different oscillations in amplitude and spatial patterns. In an experiment named (run 12c) the second normalization ratio is multiplied by a factor 1.1 for comparison with the reference (run 12a). Run 12c simulates oscillations with the

amplitude of both warm and cold peaks significantly larger. The period is slightly longer (48 months), but it is only the warm events that last much longer indeed. Out of the 48 months of a cycle, 28 have an SST Niño3 index warmer than 2°C and 8 have an index colder than -2°C. Warm events present a double-peak, sometimes a triple-peak at 3.0°C, cold events have a unique minimum at -3.5°C. The first 15 years are very regular and are analyzed hereafter. Past year 15, there are no more ENSO-like oscillations, the index stays between +2°C and +3°C. This experiment is nevertheless retained here because it reminds the reader about the great sensitivity of coupled simulations (similar change of behavior can be found for all the ICMs presented in these papers) and because investigating the mechanisms simulated by the experiment 12c that reproduces stronger warm events brings more insight.

Budgets computed as in Fig. 17 for experiment 12c (not shown) show that the thermocline displacements (term T6) in the eastern Pacific contribute to initiate the SST warming as in run 12a, but conversely to the latter the local downwelling (term T5) then contributes to the full development of the warm phase with the appearance of the second warm peak. During the second year of the warm event, advection of the anomalous zonal gradient of heat by the climatological SEC (term T2) heats up the eastern and central Pacific. These terms contribute to increase the warming once the SST anomaly in the central eastern Pacific is large enough. Thus run 12c simulates a role for terms T5 and T2 during the warm events that resembles the one simulated during the 1983 event in the forced context. These terms contribute to warming only, which explains why warm events last longer in run 12c than run 12a and cold events do not.

Figure 19 compares the wind for typical events simulated by Tsub.Astat (run 12a or 12c) with various observed ones. During cold phases, observed maximum easterlies are located at the dateline, no matter if the event is mild like in 1984 or strong like in 1976 or 1988 (Fig. 19a). During mild warm events like in 1972, 1976, 1987 or 1992 the location of the maximum westerlies is also centered in the central Pacific (Fig. 19b). By contrast,

westerlies extend east of the dateline during the strong warm events in 1983 or recently in 1997-1998. Tsub.Astat (12a) which reproduces mild events simulates westerlies with an amplitude and a position in between the observed 1987 and 1983 events and mild easterlies at the dateline during cold phases. Tsub.Astat (12c) which exhibits stronger warm and cold events, simulates intense easterlies which remain located at the same place. Similarly westerlies get stronger during warm events, but they extend eastward of the dateline as far as 140°W. Run 12c agrees remarkably well with the westerlies and easterlies observed during strong events. It is striking that increasing the normalization ratio for the second mode allows the model to reproduce the eastward extension of the westerlies in case of strong warm events as well as its steady position in case of strong cold phases. Of course, these features take place only because they grow in a coupled context. Forced by observed SST, Astat does not change much at all when the ratio of the second mode is chosen as in run 12c.

Results of the last 3 sections can be summarized as follows. On one hand, Tsub.Astat is overly sensitive to the assumptions made in the statistical atmosphere. Slight changes in the statistics can lead to the loss of oscillatory behavior or to overly large amplitudes. On the other hand, Tsub.Astat has a fairly robust behavior. It is not drastically affected by changing the coupling or the friction coefficient like Tsub.Conv. When the statistical atmosphere is modified to better match strong events, the coupled simulations better match the observed oceanic and atmospheric features in this case. Indeed run 12c has stronger off-equatorial anomalies than run 12a and when the wind anomalies are filtered out beyond 5°, the model does not oscillate anymore. This leads us to further examine the off-equatorial processes.

7. Role of the off-equatorial variability

Thermocline anomalies simulated by experiment 12c are zonally integrated and presented as a function of latitude and time for one cycle picked from the first 15 years

(Fig. 20a). The origin of time is set at the first warm peak of this cycle. Past month 0, the heat content remains negative on average for the next 30 months South of 5°N, whereas it stays significantly positive in the North. At month +25, when the Niño3 SST index starts decaying, the equatorial content has reached its minimum, due to the penetration of the upwelled South. Afterwards once the system is reversing from warm Niño3 index to cold, the Northern heat content maximum is propagating towards the equator. It continues recharging the equatorial ocean past the cold Niño3 SST peak (month +40), till the next growing warm event reaches its maximum at month +48. Interestingly past year 15 when run 12c simulates a quasi-permanent warm index, there is no intrusion of cold waters from the South, the reversal does not take place, and the North stays warm, the South stays cold, there is no more exchange between the off-equator and the equator.

These results are compared with experiment 12a (Fig. 20b). The anomalies are weaker, particularly South of 5°S. The off-equator is not necessary to reverse the warm events. Nevertheless run 12a presents very similar features to run 12c. It is striking that the North is recharged after the warm peak and that it also contributes to recharge the equatorial ocean afterwards to prepare for the next warm event. This is all the more striking as these results are specific to Tsub.Astat. CZ (see Fig. 9j in Part I) and Tsub.Conv (see Section 3, Part II) simulate the opposite sign in the North past the warm peak when both the North and the South are upwelled.

The zonally averaged thermocline variations are now presented for the observations, with the time centered on January 1983 (Fig. 20c) and on January 1987 (Fig. 20d). It is striking that following the 1983 strong event, the South is discharged like the equator while the North is recharged, consistently with what is described in Tsub.Astat. Similarity with Tsub.Astat is also observed during 1985/1986 and 1988/1989 when the equatorial heat content gets recharged from the North. In order to examine the symmetry of the variability relative to the equator, the oceanic heat content anomalies are averaged in longitude over the whole domain and between 7° and 15° of latitude and presented as a

function of time in the North or in the South (Fig. 21). On all time series, the peaks of the Niño3 SST index are indicated by vertical tickmarcks. For CZ and Tsub.Conv (Fig. 21cd), northern and southern time series are positively correlated as both the North and the South are discharged after the warm peaks. For Tsub.Astat and for observations (Fig. 21abe), time series are clearly anticorrelated. It is important to understand that it is only in a coupled mode that Tsub.Conv and CZ simulate symmetric signals. They do not in a forced context (Fig. 21f). The time series simulated by CZ have stronger amplitude because the friction is weaker, but all models CZ, Tsub.Conv or Tsub.Astat forced by observed winds reproduce the negative correlation between the Northern and Southern signals, in fair agreement with what is observed in the ocean. As explained in Part I, the coupled off-equatorial thermocline anomalies are linked to the large-scale low-frequency changes of the wind stress curl. The reasons for the northern and southern time series to be positively or negatively correlated can be found in the wind and are explained with Figures 22 and 23.

CZ simulates strong easterlies beyond 7° of latitude in the eastern Pacific (Fig. 22 adg). With the strong westerlies along the equator, they correspond to a positive (negative) curl in the North (South). These curls are associated with upwelled ocean both in the North and South as explained in Part I. Similar sign is found for Tsub.Conv (Fig. 23adg). The meridional wind does not contribute much at all to the curl for these models. By contrast, Tsub.Astat (Fig. 22beh and 23 beh) simulates very weak zonal wind anomalies northward of 5°N. It is the meridional wind component which is responsible for the off-equatorial wind stress curls. During warm events, Tsub.Astat simulates northerlies over most of the Northern Pacific with an amplitude that decays with western longitudes. It thus simulates a negative wind stress curl beyond 10°N. In the South, it is rather the zonal wind anomaly decay with latitude which is associated with the negative curl during warm events. The effect of these curls on the thermocline is negligible close to the equator if the topography of the thermocline is in Sverdrup balance with the wind, and it increases with latitude as the Coriolis factor. Tsub.Astat simulates an anticyclonic curl beyond 10°N

and a cyclonic curl in the South, which explains why the ocean is downwelled in the North and upwelled in the South. A strong event (1983) and a mild event (1992) are presented in Fig. 22cfi and 23cfi for comparison. It is clear that the observed curl is also mostly due to the meridional wind in the North whereas it is mostly explained by the zonal component in the South. This is also the case in 1987 (not shown). The signs and patterns of the wind agree remarkably well with the Tsub.Astat model.

Finally, the thermocline variations induced by Ekman pumping and the ones derived from the Sverdrup balance are computed based on Equation O1 (see Part I, section 5). The thermocline variations induced by Ekman pumping are estimated by integrating in time the wind-stress curl anomalies (after having locally removed the residual time-averages over one oscillation), and those verifying the Sverdrup balance by integrating in longitude starting from the thermocline position at the eastern boundary. The two estimates are zonally averaged in the northern and southern bands and compared to the thermocline anomalies (Fig. 24). The match with the Sverdrup balance is all the better as the curl changes are lower-frequency and the curl patterns have a wider zonal extent. Thus the ocean recharge variations simulated by experiment 12c in the North matches very well the Sverdrup balance whereas the Ekman pumping explains very little. In the South, the two estimates have similar amplitude because the curl is not as homogeneous as in the North. The zonal extent of the curl in the South is about one third of its counter-part in the North. In both hemispheres, the thermocline variations lag the Sverdrup balance by a few months because it takes time to reach the balance in the western Pacific. The variations are leading the Ekman pumping response because they are influenced by the reflection of the equatorial signal at the eastern boundary. Observations are better explained by Ekman pumping especially in the South, but in the North where the curl is extended over a wider pattern along the ITCZ, Ekman pumping does not explain at all the signal. It is not well matched either by the Sverdrup balance. The latter leads the heat content maxima in 1983

and 1992. It could then contribute to explain the thermocline variations better than the Ekman pumping.

8. Discussion and perspectives

In this study, we have examined the coupled behavior of different ICMs, mostly the CZ, Tsub.Conv and Tsub.Astat models. They all simulate oscillations of the Niño3 SST index that ressemble ENSO. Nevertheless they all have very different characteristics in amplitudes and patterns of SST, thermocline and wind anomalies and simulate very different mechanisms responsible for their oscillatory behavior.

The CZ model simulates warm events that are way stronger than in reality and inter-events with brief and weak cold events. These deficiencies do not exist in Tsub.Conv nor Tsub.Astat. Both models work really well in relocating the wind anomaly close to the dateline and in simulating the impact of thermocline displacements on the SST changes in the eastern Pacific. Compared to CZ, they both simulate wind and thermocline anomalies within 15° of the equator which agree better with observations. Moreover by modifying the parameterization according to data, both are able to reproduce some aspects of amplitude-duration- spatial patterns that change with the intensity of the events as in reality.

Deficiencies specific to Tsub.Conv are the zonal wind in the eastern Pacific and the weakness of the meridional wind anomalies. Thus even though the westerlies in the central Pacific are pretty strong and propagate with the thermocline slowly to the East like in the case of observed strong El Niño events, the spurious easterlies in the eastern basin do not allow the SST anomalies to extend eastward all the way to the South American coast as in data. They have a negative coupled feedback and make the model easily loose its oscillatory behavior. Tsub.Conv needs a friction weaker than 12 months and a coupling coefficient increased by 20% to oscillate. This is a concern because the model clearly overestimates the role of Rossby waves and the wind stress curl in the North which is associated with the reversal of the zonal wind component with latitude and is not found in data.

Tsub.Astat has a relatively more robust coupled behavior. The simulated winds agree really well with the observed ones. ENSO-like oscillations are obtained with a friction equal to 9 months or weaker, and are not much sensitive to the coupling coefficient. The model simulates realistic off-equatorial zonal and meridional wind as well as thermocline anomalies. Weakening the friction does not increase the amplitude of the thermocline displacements as it does in Tsub.Conv. With a friction of 9 months, warm events last longer than with a friction of 12 months. In a mild coupling context, the coupled variations are relatively confined to the equator in comparison with CZ or Tsub.Conv and the model can oscillate with the 5 gravest Rossby modes only.

One of the key mechanisms involved in triggering and reversing the oscillations simulated by these ICMs is the coupling between the off-equatorial and equatorial system: the SST anomalies sustain large wind curl anomalies in the off-equatorial Pacific that are associated with steep zonal slopes of the thermocline. By reflection at the meridional boundaries and by continuity in the interior of the domain, high Rossby modes influence the recharge and discharge of the equatorial heat content. Only CZ looses its oscillatory behavior when the Kelvin mode is not allowed to reflect in Rossby modes higher than 5 at the eastern boundary, but all models are sensitive to the reflection of Rossby modes higher than 5 at the western boundary. CZ and Tsub.Conv systematically loose their oscillatory behavior without it. Tsub.Astat is less dependent on off- equatorial physics when it is in a mild coupling context, the off-equator then contributes only to lengthen the period of oscillations. In a strong coupled case, Tsub.Astat looses its oscillatory behavior like Tsub.Conv and CZ. The way the meridional mass adjustment takes place in Tsub.Astat is quite different from the other two models. CZ and Tsub.Conv simulates a discharge of the whole ocean after the warm peak, because of the spurious off-equatorial easterlies that are associated with the pair of cyclonic curls on both sides of the equator. For Tsub.Astat, the North gets recharged and the South discharged after the warm peak. The South drags heat away from the equator and reverses the growing event, then the North starts re-filling the

equator for the next warm event to grow. The anticorrelation between the North and the South is due to the asymmetry of the wind anomalies which is well reproduced by the statistical atmosphere with the equatorial westerlies stronger South of the equator than North and the northerlies stronger along the ITCZ than the southerlies South of the equator. Therefore, the charge in the North corresponds to the anticyclonic curl associated with the northerlies in the Central Pacific that decay towards the West and the discharge in the South corresponds to the cyclonic curl associated with the equatorial westerlies that decay away from the equator. The North gets all the more recharged and the South all the more discharged as the warm event lasts long and the westerlies penetrate eastward.

Some of the questions raised in the introduction of this study (Part I) can be addressed with these ICMs to the extent that they reproduce relatively realistic ENSO-like events. One is relative to why are some events stronger than others. Another one is about the differences between cold and warm events. According to observations, the strongest warm events correspond to westerlies that extend more eastward in the Central Pacific than during mild events. This is well reproduced by experiments forced by observed winds over the 1980-1997 period. One of the main results of this paper is that this feature is also successfully reproduced in a coupled context with Tsub.Conv and Tsub.Astat. Both models have the capacity of simulating stronger warm events (that have a bigger amplitude and last longer), when the wind anomaly is located further east. This is obtained by decreasing the weight of the atmospheric convection relative to the local heating in Conv component, or by slightly increasing the normalization ratio of the second wind SVD eigenvector in Astat. Because this allows to emphasize the "slow" SST mode of growth in the eastern Pacific, it is also associated with a stronger role of the off-equatorial ocean-atmosphere in the coupled behavior.

Cold events are not the opposite picture of warm events. According to observations, the coldest anomalies are always located in the central Pacific, never along the American coast and the maximum easterlies are at the dateline or west of it, but never

significantly east of it. They are associated with thermocline downwelling in the west and westward current anomalies that advect cold waters from the central Pacific to the warm pool. The mechanisms at work in the western Pacific depend a lot more on baroclinic changes than on local coupling between the SST and the wind. The coupled experiments reproduce similar characteristics. The simulated cold SST maxima are located at 130°W and the wind maxima at the dateline. The baroclinic current and thermocline anomalies have competing roles on the SST in the western Pacific. The thermocline downwelling is efficient to reverse the growing cold event because the easterlies are associated with an anomalous upwelling that adds up to the climatological rate. The zonal transport of cold and the vertical transport of heat have a net impact on the SST changes which is weak. Therefore, the warm pool is not cooled down enough to further reinforce the easterlies. Cold events happen via a "fast" coupled mode of growth in the central-western Pacific. Changing the strength of the atmospheric convection or the second SVD affects the amplitude of the cold events, but does not change their duration nor the location of the easterlies. It is quite remarkable that in case of strong coupling, the 30 year averaged simulations have a tendency to be biased towards warm events while in a forced context both the ocean and the atmosphere models privilege the cold events. This happens because of the privileged "slow" SST mode of growth for warm events and "fast" baroclinic mode of growth for cold events.

The question of what triggers the warm events is far from being fully addressed with these ICMs. The recharge of the equatorial heat content by the off-equatorial coupled system is certainly active in the ICMs, but this does not mean that in reality it takes place like the models simulate it. CZ is triggered by thermocline downwellings in the Southwestern Pacific, that are irrealistically large and generated by wind stress curls in the Southeastern Pacific that are not found in reality. Tsub.Conv displays similar processes, except that the thermocline downwelling rather take place in the North than in the South. Both correspond to a slow mass adjustment after recovery of the global upwelling induced

by the warm event. Tsub.Astat recharge from the North correspond to a slow mass adjustment where the heat accumulated in the North after the warm peak propagates towards the equator as the northerlies get closer to the equator. Indeed some similarity can be found with observations and with the scenario proposed by Wyrtki (1985) and Jin (1997). However Nature is not as systematic as the scenarii reproduced by models and the recharge can also be performed by the South as observed prior to 1992 for instance. In addition, the recharge may be a necessary condition for an event to grow, but this does not mean that it is a sufficient condition. The coupled simulations do not reproduce the westerly wind bursts which may play a significant role in triggering warm events (e.g. Barnett, 1984). Indeed CZ, Tsub.Conv and Tsub.Astat all miss the variability of the wind West of the dateline.They also all miss the lead of the Niño4 TX index relate to Niño3 SST. For this purpose, using an atmospheric model which is not a slave model is necessary. Such an example coupled to the CZ ocean is proposed in (Kleeman, 1997).

One deficiency common to Tsub.Astat and Tsub.Conv is the lack of variability of the thermocline in the Central equatorial Pacific. A solution may consist in adding higher baroclinic modes in the ocean model because such modes would not propagate the variability as far away from the region of strong wind anomalies (Chen and Sarachik, 1995). But the minimum of variability in the central Pacific is not only due to the deficiency of the ocean model since in a forced mode, Tsub.Astat and Tsub.Conv reproduce reasonably well the thermocline variability in the equatorial band. Coupled models select a location and a frequency associated with their strongest mode of growth which becomes dominant. The thermocline has thus a node of variation in the Central Pacific where the low-frequency wind changes take place and oscillate between quasi-balanced states with the zonal wind along the equator. Although the models do simulate thermocline displacements in the eastern Pacific leading by a few months the growth and decay of the warm events, these ICMs are far from reproducing the diversity of phase shifts between the SST, the thermocline and the wind signals that are observed or simulated by the forced experiments

in the various regions of the equatorial Pacific. It is possible that adding the wind noise derived from the variance of the observed wind variability left after SVD in a coupled Tsub.Astat experiment helps recover a wider spectrum as demonstrated in (Blanke et al, 1997). Another possibility is to try and reduce this privileged mode of growth. Tsub.Conv and Tsub.Astat models both tend to overestimate the positive feedback between the SST in the eastern Pacific and the wind in the Central Pacific that locally induces downwelling which dominates over all the other mechanisms that can affect the SST. Following observations, one may want to introduce a mixed layer deeper in the Central Pacific than in the East in order to reduce the role of term T5 there. Indeed coupled results are highly sensitive to the prescribed climatological fields which need to be revisited as well. In addition it may be worth introducing a time dependance of the mixed layer depth as it varies with the season and the interannual events. These questions are under investigation.

Finally these ICMs suffer from the lack of physics in the simulation of the air-sea flux exchanges at the interface. The ocean mixed layer looses heat during warm events or gain heat during cold events via the damping term. Although this term has some resemblance with the heat released to the atmosphere (Seager, 1992), one should not forget that in reality, air-sea fluxes are a lot more complex than damping. Latent heat is particularly sensitive to the wind speed rather than the SST. Its role is important during cold events because trade winds are stronger than normal and enhanced evaporation contributes to cool down the ocean. Conversely during warm events, the trade winds can be so much weaker than normal that wind speed is lower than the threshold of evaporation. Adding net air-sea heat fluxes derived from observations in the "control run" significantly affects the SST (see DP96) and one can expect that the coupled system is highly sensitive to such positive feedbacks. Indeed the ICMs presented above oscillate between warm and cold anomalies without staying for several years in a quasi-normal state as in Nature during interevents. Introducing a coupled mechanism (like latent heat) that has a positive feedback

and that depends on a threshold should reduce this deficiency. This question is under investigation.

Obviously models with more physics for the ocean, the atmosphere and the coupling are necessary to reproduce the complexity and variety of the actual ENSOs in the tropical Pacific. Nevertheless our goal was only to understand some aspects of this variety and be able to reproduce them with a coupled model. Using data to revisit the CZ model has considerably improved the agreement between the observed variability of the thermocline, wind and SST and the one simulated over 30-year long coupled runs. It is worth examining the ENSO forecasting skill of both models in comparison to CZ (manuscript in preparation). Forced by observed SST, Tsub.Astat reproduces really well the details of the SST, wind and thermocline anomalies over a period different from the one which has been used to determine the statistical atmosphere. Thus performance in terms of predictions should not be limited by the statistical approach itself. To the extent that westerly wind bursts are well observed by the wind data used to drive the model and initialize forecasts, Tsub.Astat and Tsub.Conv should not either drastically suffer from underestimating the wind variability in the western Pacific. However, forecasts are exposed to a wide variety of initial conditions that affects the transition between forced and coupled behavior. One should not expect that conclusions drawn from 30 year long runs apply directly to series of two-year long forecasts. In any case, being aware of the models capacities and deficiencies in reproducing the observed ENSO variability certainly helps understand the successes and failures of forecasts.

Acknowledgements: The authors at the Jet Propulsion Laboratory, California Institute of Technology were supported under contract with the National Aeronautics and Space Administration. They thank Drs S. Zebiak and M. Cane from Lamont Doherty Earth Observatory for providing their code of the coupled ocean-atmosphere model, input files, initialization procedure as well as their time and helpful discussions.

Bibliography

Barnett T.P, 1984: Interaction of the monsoon and Pacific trade wind systems at interannual time scales. Part III: A partial anatomy of the Southern Oscillation. *Mon Wea. Rev.*, 112, 2388-2400.

Battisti, D. S., 1988: Dynamics and thermodynamics of a warming event in a coupled tropical atmosphere-ocean model. *J. Atmos. Sci.*, **45**, 2889-2819.

Battisti D. S., 1989: On the role of off-equatorial waves during ENSO, *J. Phys. Oceanogr*, **19**,551-559.

Blanke B., D. Neelin and D. Gutzler, 1997: Estimating the effect of stochastic wind stress forcing on ENSO irregularity., *J. Climate*, **10**, 1473-1486.

Chao, Y. and G. S. Philander, 1993: On the structure of the Southern Oscillation. J. Climate, Vol 6, n°3, 450-469.

Chen Y.Q., D.S. Battisti, and E.S.Sarachick, 1995: A new Ocean Model for studying the tropical Oceanic aspects of ENSO, *J. Phys. Oceanog.*, **25**, 2065-2089.

Dewitte B. and C. Perigaud, 1996: El Niño - La Niña events simulated wth the Cane and Zebiak's model and observed with satellite and in situ data. Part II: model forced by data, *J. Climate*, **9**, 1188-1207.

Gill, A.E., 1980: Some simple solutions for heat induced tropical circulation. *Q. J.R.Meteor. Soc.*, **106**, 447-462.

Jin F.F., 1997: An equatorial Ocean recharge paradigm for ENSO. Part I: Conceptual Model, *J. Atmos. Sc.*, **54**, 811-829.

Kirtman B.P.and S.E. Zebiak, 1997: ENSO simulation and prediction with a hybrid coupled model, *Mon. Wea. Rev.*, **125**, 2620-2641.

Perigaud C, S. Zebiak, F. Melin, JP Boulanger and B. Dewitte, 1997: On the role of the meridional wind anomalies in a simple model of ENSO, *J. Climate.*, **10**, 761-773.

Picaut, J. F. Masia, and Y. du Penhoat, 1996: An Advective-Reflective conceptual Model for the Oscillatory Nature of the ENSO, Science, **277**, 663-666.

Seager R., 1989: Modeling Tropical Sea Surface Temperature: 1970-1987. J. Phys Oceanog., 19, 419-431.

Syu H.H., J.D.Neelin, and D.S.Gutzler, 1995: Seasonal and interannual variability in a hybrid coupled GCM, *J. Climate*, **8**, 2121-2143.

Wyrtki K., 1985: Water displacements in the Pacific and the genesis of El Nino cycles, J. Geophys. Res., **90**, 7129-7132.

Zebiak, S. E., and M. A. Cane, 1987: A model El Niño-Southern Oscillation. *Mon. Wea. Rev.*, **115**, 2262-2278.

Table 1: Identification of the Tsub.Conv and Tsub.Astat coupled experiments

MLO=Mixed Layer Ocean component, in which Tsub parameterization is used.
fric= decay time of the Rayleigh friction in months.
coupling= ratio between the drag used in a coupled and forced experiment.

Id	MLO	Atmos	fric	coupling
1a	CZ	CZ	30	1.645
3a	Tsub	Conv	30	1.645
4	Tsub	Conv	6	1.645
5	Tsub	Conv	6	1.645 * 1.2
6	Tsub	Conv	15	1.645 * 1.2
7a	Tsub	Conv	12	1.645 * 1.2
8	Tsub	Astat	6	1.0
9	Tsub	Astat	6	1.2
10	Tsub	Astat	12	1.0
11a	Tsub	Astat	12	1.2
12a	Tsub	Astat	9	1.0

Runs 7bew, 11b and 12bwic have the same parameterizations as run 7a, 11a and 12a respectively.
Runs 7b, 11b and 12b correspond to filtering the wind beyond 9°N and 9°S before time-stepping baroclinic and MLO as in run 1b of Part I.
Run 7w and 12w correspond to filtering out Rossby modes higher than 5 before reflecting into Kelvin at the western boundary as in run 1e of Part I.
Run7e allows Kelvin to reflect only into the 5 gravest Rossby modes at the eastern boundary as in run 1f of Part I.
Run12i retains only the Kelvin and the 5 gravest Rossby modes in the whole baroclinic ocean model.
Run 12c has the normalization ratio of the second SVD eigenvector multiplied by 1.1.
Tsub.Astat(run 0) is the run forced by the CAC SST anomalies.

Table 2: Tsub.Conv coupled experiments testing the role of atmospheric convection

Tsub.Conv Runs (3*) correspond to the parameterization defined in run 3a, except for the ratio of the convection term over the local heating that both drive the atmospheric model.

Ratio	Run Id	Period	Amplitude
0.	Tsub.Gill	52	2.0
0.25	3b	48	1.7
0.75		45	1.6
1.00	3a	36	1.4
1.25		33	1.1
1.50		31	0.8
1.75	3c	30	0.6

Period is the number of months between two warm peaks of the Niño3 index simulated over the 30 year long runs, amplitude is their standard deviation in Degrees Celsius.

Appendix: Non linearities in Tsub.Conv and Tsub.Astat

Role of climatological background

The terms that involve the climatology are in the mixed layer, in the forcing of the atmosphere and in the transformation of wind into wind stress anomalies as follows:

1) in the mixed layer (see Equation T in Part I)

* zonal advection:

-	U	x	$(\underline{T}+T)_x$	(T1)
+	$\underline{U}$	x	$(T)_x$	(T2)

* meridional advection:

-	V	x	$(\underline{T}+T)_y$	(T3)
+	$\underline{V}$	x	$(T)_y$	(T4)

* vertical advection:

$-\gamma_1$	{M(WT)-M($\underline{W}$)}	x	$\underline{T}_z$	(T5)
-	γ_2 M(WT)	x	(T-Tsub)/H1	(T6)

(T1) is large in the western and Central Pacific as U is strong there and not in the East because of the conditions of reflection at the Eastern boundary. T1 is stronger during cold rather than warm onsets, because Tx weakens $\underline{T}x$ in case of warm event.

(T2) is significant only in case of strong warm events after the onset and in the Central-Eastern Pacific: it transports anomalous warm waters back to the warm pool.

(T3) is significant only in the South eastern Pacific and contributes to the southward extension of warm anomalies, including the SST maximum along the coast South of the equator. The cold tongue waters are located South of the equator and T3 heats up the system when the meridional current anomalies are southward during the onset of warm events.

(T4) is significant at the equator and north of it to export heat towards the North during warm events after the onset, because $\underline{V}$ is northward at the equator in the Eastern Pacific.

(T5) is the dominant term in central Pacific where anomalous Ekman downwelling is stronger than the climatologic upwelling rate.

(T6) is affected by 3 terms, the total upwelling rate, the subsurface temperature Tsub that varies with thermocline displacements and the surface temperature T. Except for the case where Tsub anomaly is smaller than the SST (see Part I), term T6 has a cooling impact in case of upwelled thermocline and a warming impact in case of downwelled thermocline. In the Central and Western Pacific, term T6 is more efficient to warm up than to cool down the system, because a downwelled thermocline corresponds to cold events and easterlies associated with local Ekman divergence that adds up to the climatological upwelling rate to advect the subsurface temperature change Tsub. Conversely the impact of an upwelled thermocline in the Central and Western Pacific is weak because the cooling of the subsurface temperature is advected at a reduced upwelling rate. In the eastern Pacific, results are even more complex. They are different north and south of the equator because the climatological upwelling changes sign, they depend on the model (CZ, Tsub.Conv or Tsub.Astat) and the forced or coupled context of the experiment because spurious wind anomalies can grow there.

All these terms play different roles in the assymetry between warm and cold events. Forced by a given amplitude of wind stress anomaly located at the dateline, Tsub ocean model simulates SST anomalies that are larger if the wind anomaly blows westward (cold event) than if it blows eastward (warm event).

2) in the forcing of the atmosphere (see Equation A1 in Part I):

$$Q_T = \alpha T \exp [(T -30) / 16.7 \} \qquad \text{:Eq A1}$$

Because the cold events correspond to SST anomalies that are located in the Central Pacific rather than in the Eastern Pacific, Equation A1 gives more atmospheric forcing in the western Pacific warm pool region than in the eastern Pacific cold tongue for equal SST amplitude. Thus the Conv model simulates easterlies in 1988 that are stronger than the

westerlies in 1987 in agreement with observations (see Dewitte and Perigaud, 1996, named DP96).

3) in the conversion of wind anomaly into wind stres anomaly:

$$TX = \rho\, Cd\, [\; WaT\, (\underline{Ua} + Ua) - \underline{Wa}\, \underline{Ua}\;]$$

$$TY = \rho\, Cd\, [\; WaT\, (\underline{Va} + Va) - \underline{Wa}\, \underline{Va}\;]$$

where WaT and $\underline{Wa}$ are the total and climatological wind speeds.

Because of the mean trade winds in the Central equatorial Pacific, the same amplitude of SST anomaly gives westerlies and equatorward convergence if it is warm that are weaker than the easterlies and the divergence if it is cold. The role of the climatology is not big on the meridional component which is much weaker than the zonal one in CZ and Conv.

In summary, it is remarkable that for an equally strong warm or cold forcing, the climatology tends to privilege the cold events over the warm ones in both the atmosphere and the ocean models.

Figure Caption

Figure 1: Time series of SST Niño3 anomalies (a), TX Niño4 anomalies (b) and H anomalies over Niño3 (c) or NiñoW (d) simulated by the 30 year long coupled runs of the Tsub.Conv (run3a). Figure to be compared with Figure 1 and Figure 3 in Part I.

Figure 2: Standard Deviation of the SST in Degree Kelvin **(a)**, the zonal and meridional wind stress in Dyn/cm^2 **(bc),** or the thermocline depth in m **(d)** simulated by Tsub.Conv (run 3a). Figure to be compared with Figure 2 and Figure 4 in Part I.

Figure 3: Standard deviation of observed and simulated SST (top) or zonal wind stress (bottom) anomalies as a function of longitude along the equator. Plots are derived from 27 years of observed anomalies (CAC SST or FSU wind stress) or from the 30 years of coupled runs for CZ or Tsub.Conv. See Tables 1 and 2 for run identification.

Figure 4: Rate of SST changes in °/month simulated by Tsub.Conv (run 3a) averaged along the equator in the western Pacific (160°E-160°W), central Pacific (160°W-120°W) and eastern Pacific (120°W-80°W) as a function of time in years. Thick line corresponds to local rate of change + damping (term T7). Thin line corresponds to anomalous upwelling (term T5), dotted line to thermocline displacements (term T6), dashed line to horizontal advection (terms T1+T2+T3+T4). See Equation T in the Appendix. Figure to be compared with Figure 7 in Part I.

Figure 5. Time series of SST Niño3 index simulated by Tsub.Conv model during 30 year long coupled runs for various values of friction and coupling coefficients and for various off-equatorial filters. See Table 1 for run identification. Figure to be compared with Figure 6 in Part I.

Figure 6: Standard deviation of observed and simulated thermocline anomalies as a function of latitude along the dateline (top) or wind stress curl anomalies as a function of longitude along 9°N (bottom). Plots are derived from 15 years of T400 or from 27 years of FSU wind stress data or from the 30 years of coupled experiments. See Table1 for run identification. Figure to be compared with Figure 14 in Part I.

Figure 7: Hovmoeller diagrams of anomalies simulated by Tsub.Conv (run 7a). Vertical axis is time in month where month zero is centered on the warm peak of year 13. Units are meters for thermocline, 10^{-8} Pa/m for wind stress curl, Degree Kelvin for SST and Dyn/cm^2 for zonal wind stress. Figure to be compared with Figure 9 in Part I.

Figure 8: Same as Fig.7 for the observed anomalies. Month 0 is January 1983.

Figure 9: Time series of SVD mode 1 **(a)** and mode 2 **(b)** for SST (plain) and wind stress (dotted). Plots **(c)** represent the SST Niño3 indices derived from the CAC data (plain) or from the sum of the 7 first SVD modes (dotted). Plots **(d)** represent the Niño4 TX index derived from the "detrended" FSU data (plain) or the sum of the 7 first SVD modes (dotted), or the Astat simulations forced by CAC data (dashed).

Figure 10: First two SVD eigenvectors for the SST **(ab)**, zonal wind **(cd)** and meridional wind stress **(ef)**. Values are normalized by their respective variance over the domain between 1980 and 1995.

Figure 11: Variability over 1980-1995 of the SST, zonal and meridional wind stress anomalies simulated by Astat forced by CAC observations. The reconstructed fields have all been multiplied by a coefficient 1.2 which is then considered as the reference drag coefficient. Units are Degrees Kelvin and Dyn/cm^2.

Figure 12: Time series of SST Niño3 index simulated by Tsub.Astat model during 30 year long coupled runs for various friction and coupling coefficients and for various off-equatorial filters. See Table 1 for run identification. To be compared with Figure 5.

Figure 13: Standard deviation of anomalies simulated by Tsub.Astat for various friction or coupling coefficients. See Table 1 for run identification. Figure to be compared with Figures 3 and 6.

Figure 14: Standard deviation of the SST anomalies in Kelvin **(a)**, zonal and meridional wind stress in Dyn/cm^2 **(bc)**, or thermocline depth in meter **(d)** simulated by Tsub.Astat model (run 12a). To be compared with Figures 2 and 4 in Part I or to Figure 2 in Part II.

Figure 15: Hovmoeller diagrams for anomalies simulated by Tsub.Astat (run12a). Month zero corresponds to warm peak of year 16. Compare with Figure 7.

Figure 16: Same as Figure 15 for observed anomalies. Month zero is January 1987.

Figure 17: Same as Figure 4 for Tsub.Astat (run 12a) on the left panels (**a1, b1, c1**), and for Tsub.Astat (run 0) on the right panels (**a2, b2, c2**).

Figure 18: Time series of SST Niño3 index or Niño4 zonal wind stress index derived from observations or Astat forced by observed SST. The eigenvectors are derived from the SVD over 1980-1995 for plots (**ab**) or from the SVD over 1970-1980 for plots (**cd**). Plots **a (b)** correspond to the CAC (FSU) data over 1970-1980 (plain) or the Astat simulations (dotted) forced by CAC data over 1970-1980. Plots **c (d)** correspond to the CAC (FSU) data over 1980-1995 (plain) or the Astat simulations (dotted) forced by CAC data over 1980-1995.

Figure 19: Zonal wind stress anomalies as a function of longitude along the equator for cold (top) or warm (bottom) peak events. Plots are derived from Astat simulations forced with CAC SST over (1970-1980) or over (1980-1995) and from the 30 year long coupled simulations of Tsub.Astat (run12a, or 12c).

Figure 20: Hovmoeller diagrams of the zonally averaged thermocline anomalies (in meters) as a function of latitude and time for Tsub.Astat simulations and observations. Time origins are centered at the warm peaks of the SST Niño3 index, i.e the first peak of the event on year 6 for run 12c, the warm peak on year 16 for run 12a, January 1983 and January 1987 for observations.

Figure 21: Time series of thermocline anomalies averaged over 130°E-80°W between 7°N and 15°N (plain) or 7°S and 15°S (dotted). Vertical marks indicate the times of the Niño3 SST peaks.

Figure 22: Maps of zonal, meridional and wind stress curl anomalies on average during the warm peaks. Maps are derived from CZ (run 1a), Tsub.Astat (run12c) and the 1983 observed event. Units are dyn/cm^2 and 10^{-7} Pa/m.

Figure 23: Same as Fig. 22 for Tsub.Conv (7a), Tsub.Astat (12a) and the 1992 event.

Figure 24: Time series of thermocline anomalies averaged over 130°E-80°W between 7°N and 15°N (left panels) or 7°S and 15°S (right panels). The three plots per panel correspond to the actual thermocline (plain) or the one derived from Ekman pumping (dotted) or the one in Sverdrup balance (dashed). Vertical marks indicate the times of the Niño3 SST peaks.

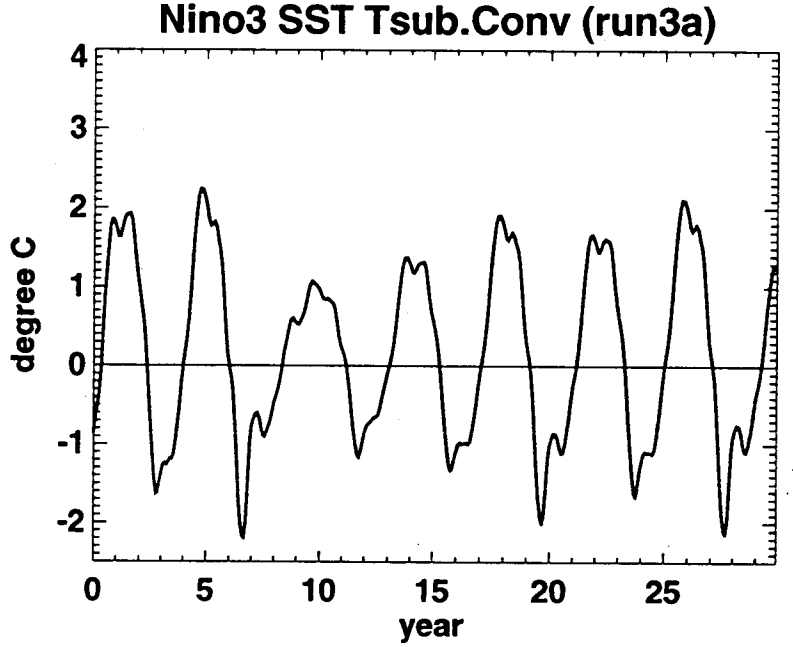
Nino3 SST Tsub.Conv (run3a)
degree C
4
3
2
1
0
-1
-2
0
5
10
15
20
25
year

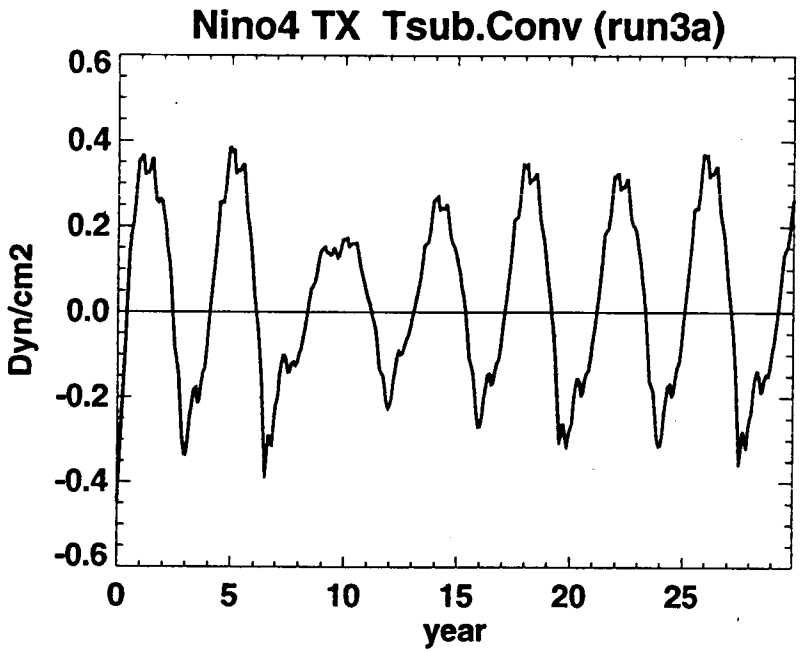
Nino4 TX Tsub.Conv (run3a)
Dyn/cm2
0.6
0.4
0.2
0.0
-0.2
-0.4
-0.6
0
5
10
15
20
25
year

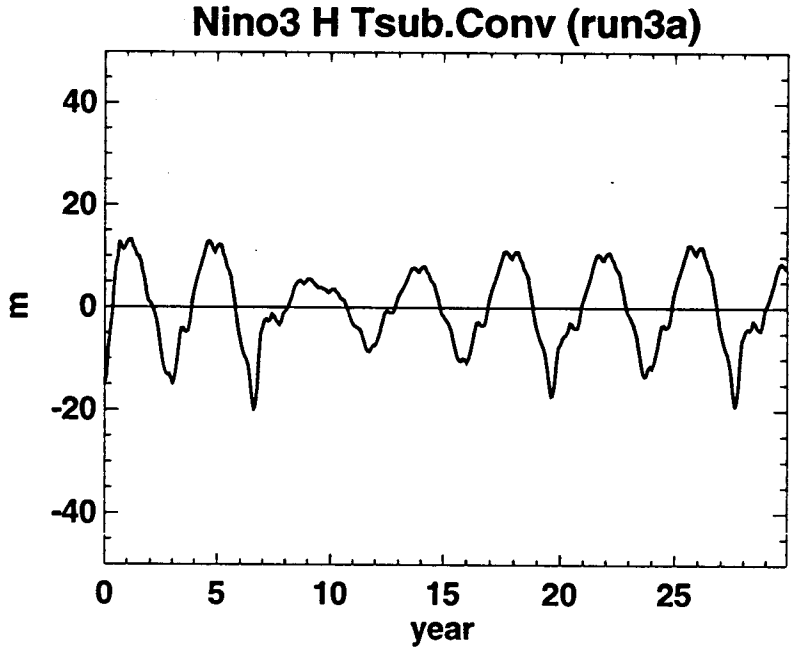
Nino3 H Tsub.Conv (run3a)
m
40
20
0
-20
-40
0
5
10
15
20
25
year

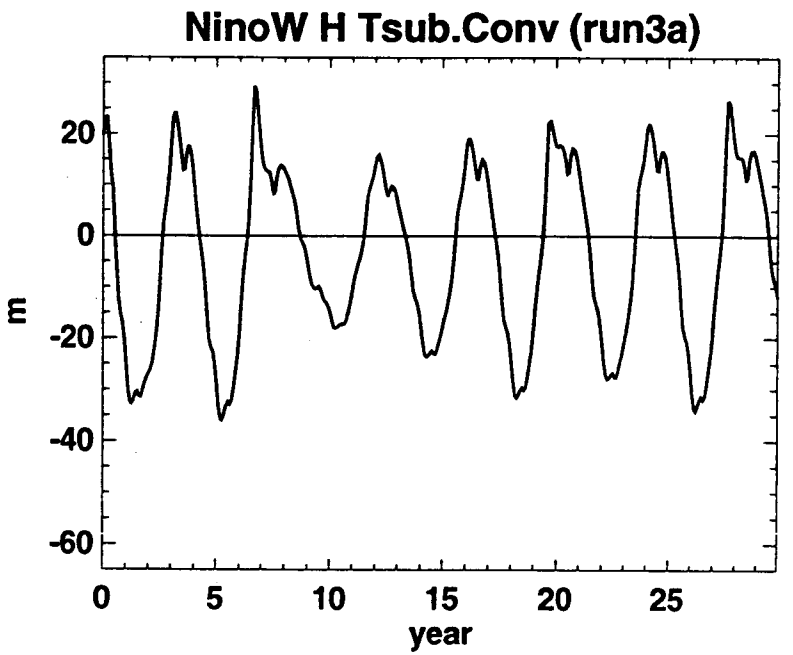
NinoW H Tsub.Conv (run3a)
m
20
0
-20
-40
-60
0
5
10
15
20
25
year

Fig.1

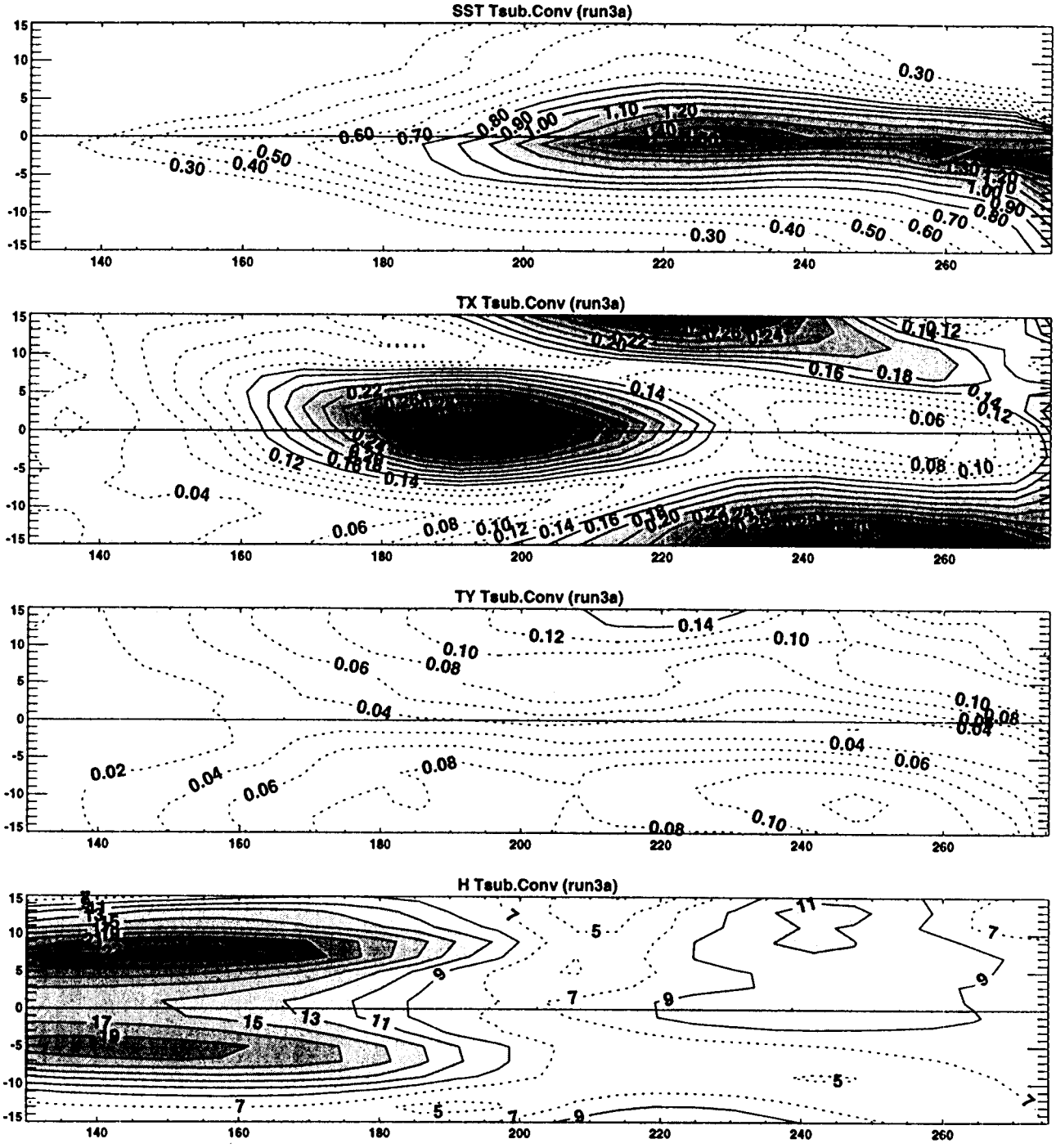
SST Tsub.Conv (run3a)
TX Tsub.Conv (run3a)
TY Tsub.Conv (run3a)
H Tsub.Conv (run3a)

Fig.2

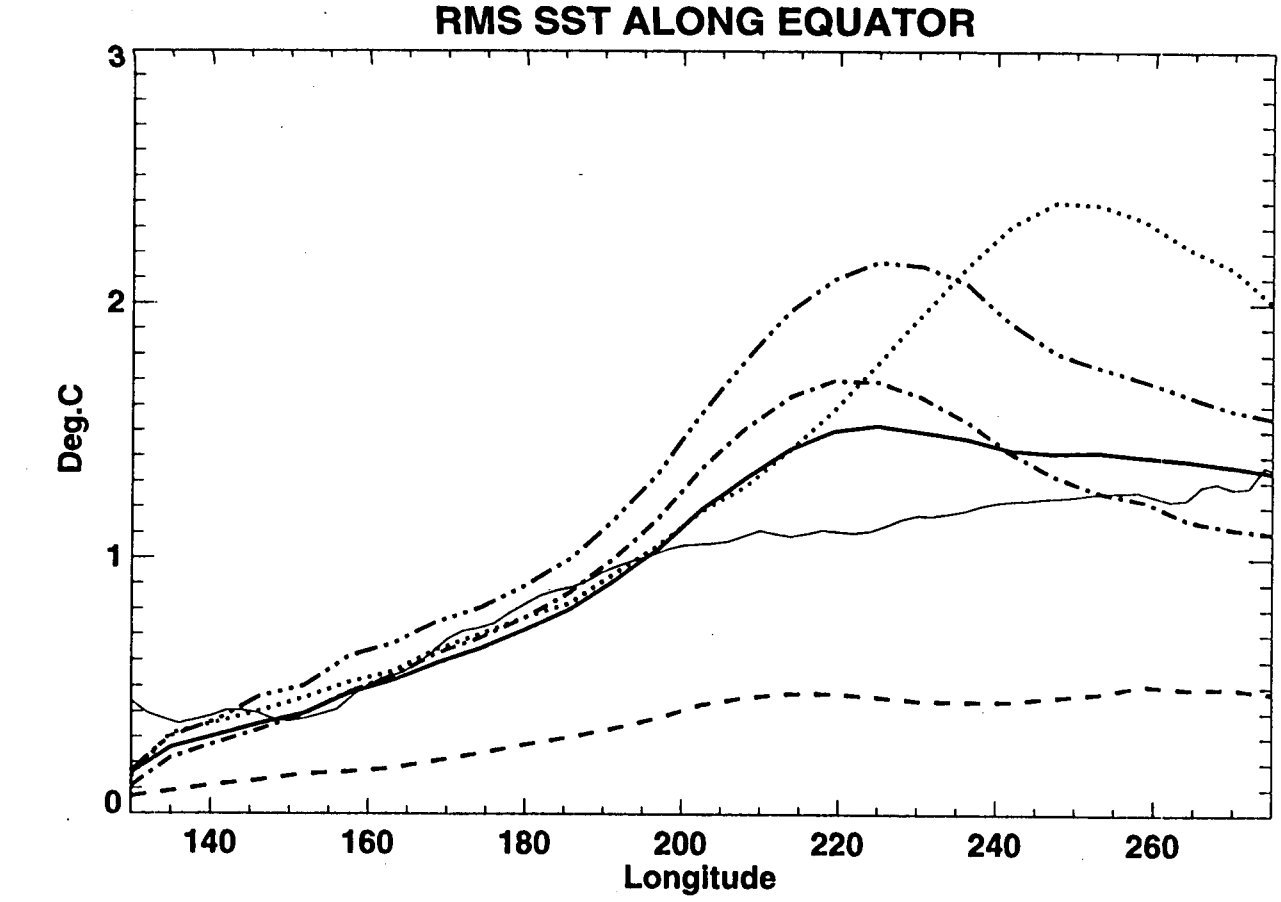
RMS SST ALONG EQUATOR
Deg.C
3
2
1
0
140
160
180
200
220
240
260
Longitude

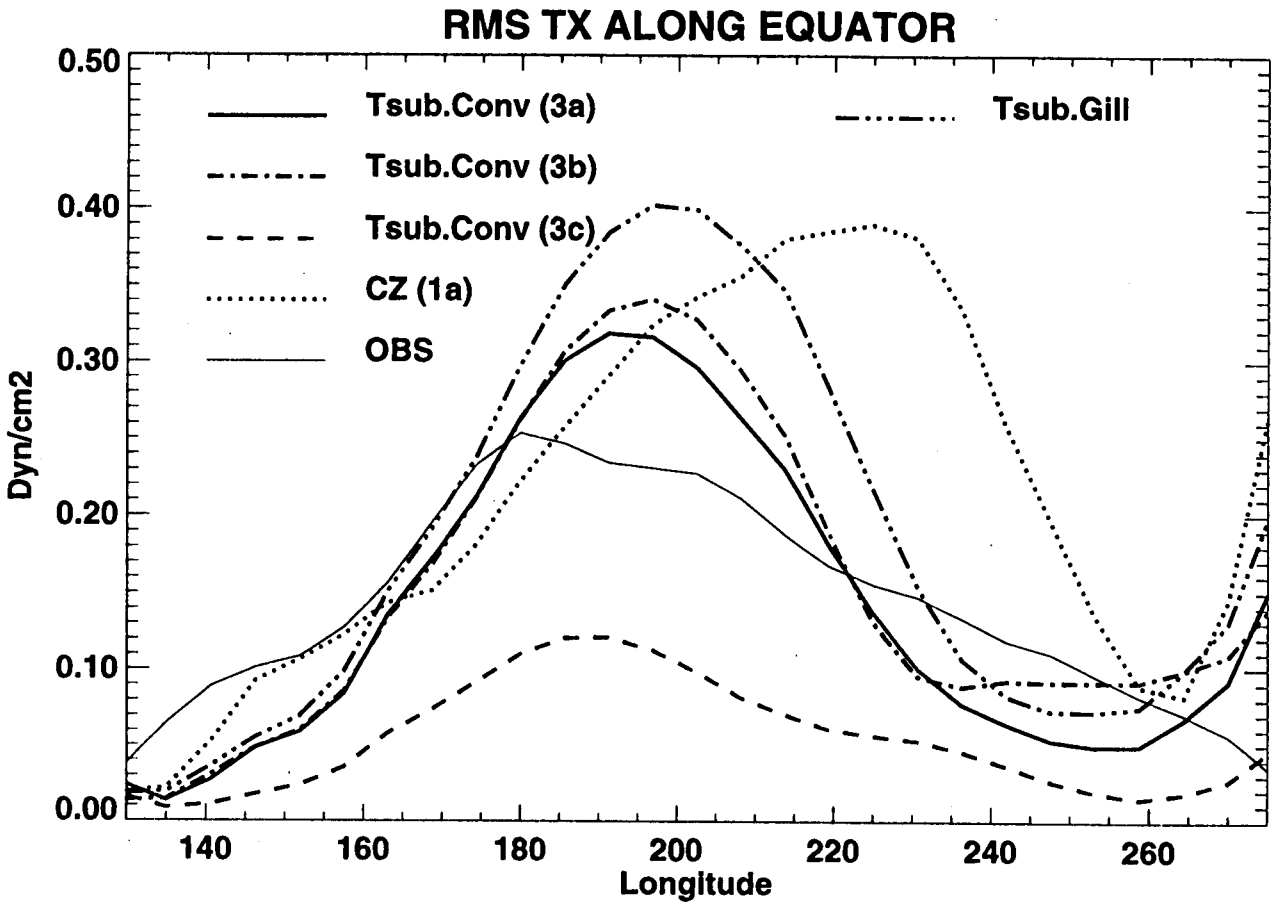
RMS TX ALONG EQUATOR
Tsub.Conv (3a)
Tsub.Conv (3b)
Tsub.Conv (3c)
CZ (1a)
OBS
Tsub.Gill
Dyn/cm2
0.50
0.40
0.30
0.20
0.10
0.00
140
160
180
200
220
240
260
Longitude

Fig.3

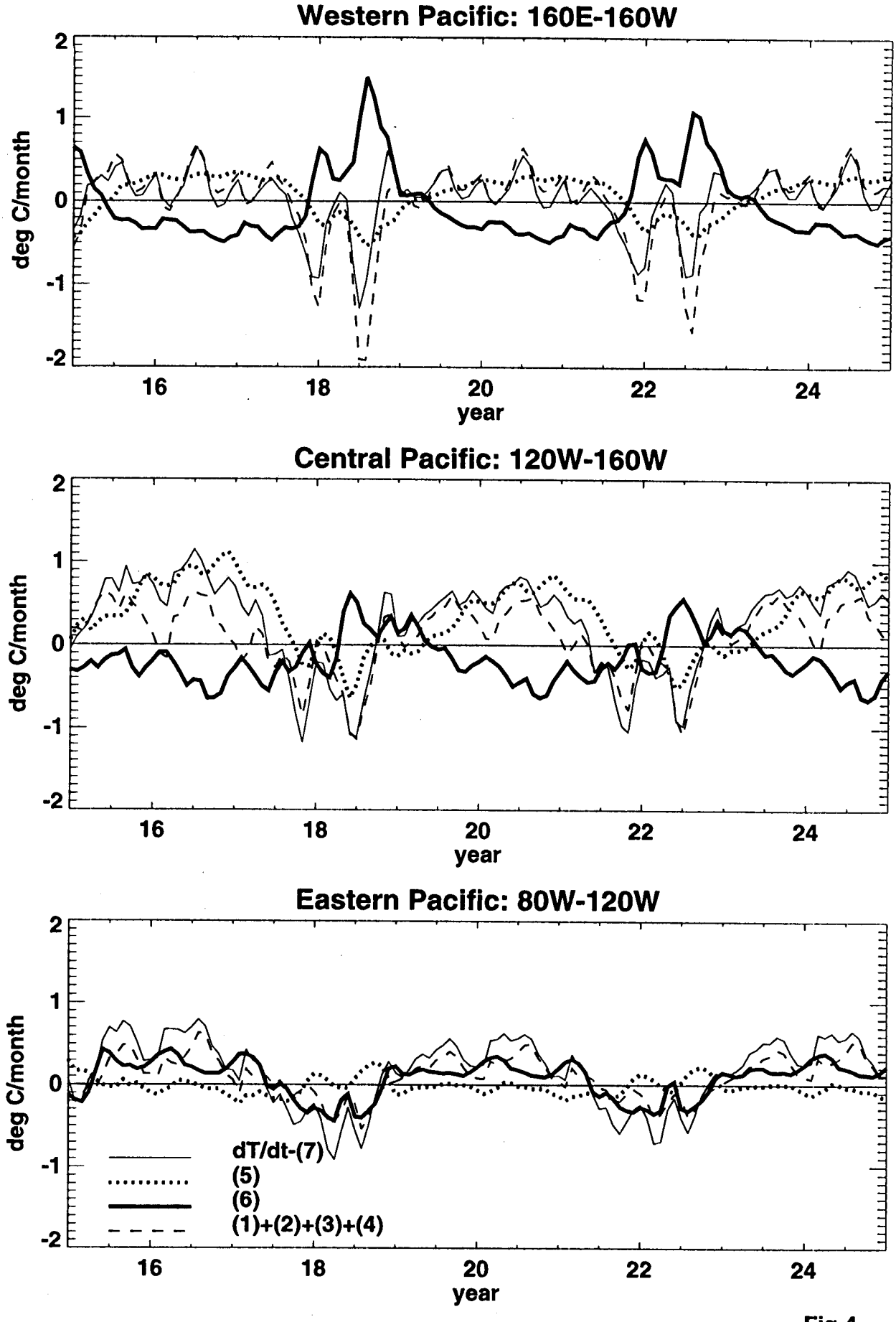
Western Pacific: 160E-160W
deg C/month
year
Central Pacific: 120W-160W
deg C/month
year
Eastern Pacific: 80W-120W
deg C/month
year
dT/dt-(7)
(5)
(6)
(1)+(2)+(3)+(4)

Fig.4

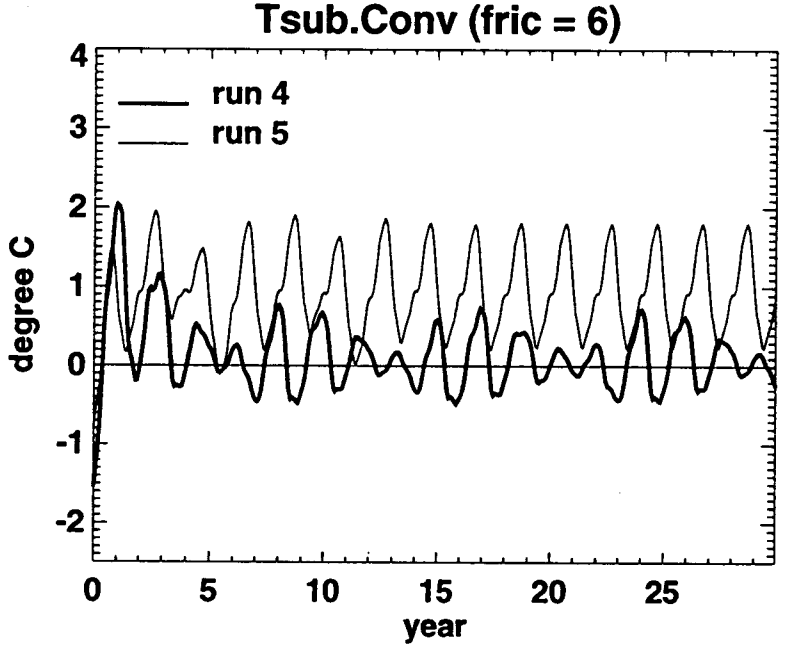
Tsub.Conv (fric = 6)
run 4
run 5
degree C
year

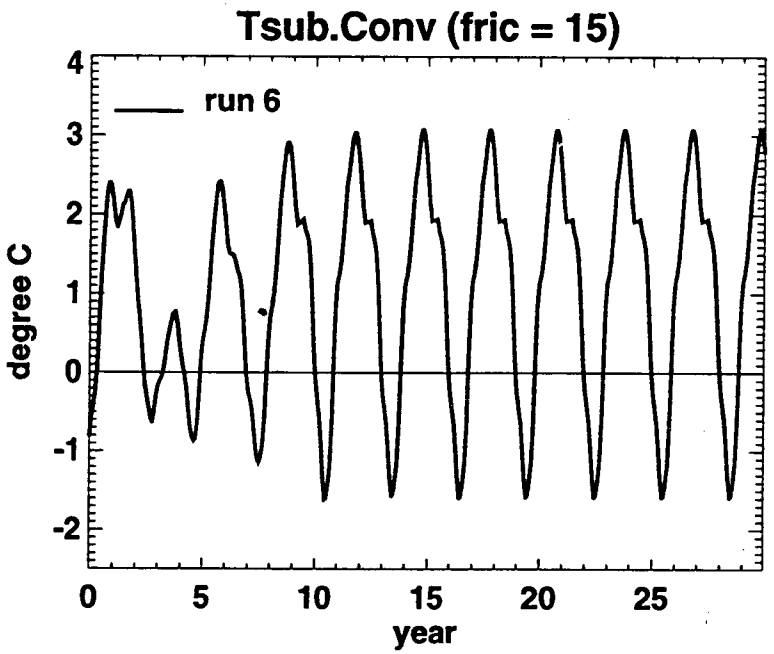
Tsub.Conv (fric = 15)
run 6
degree C
year

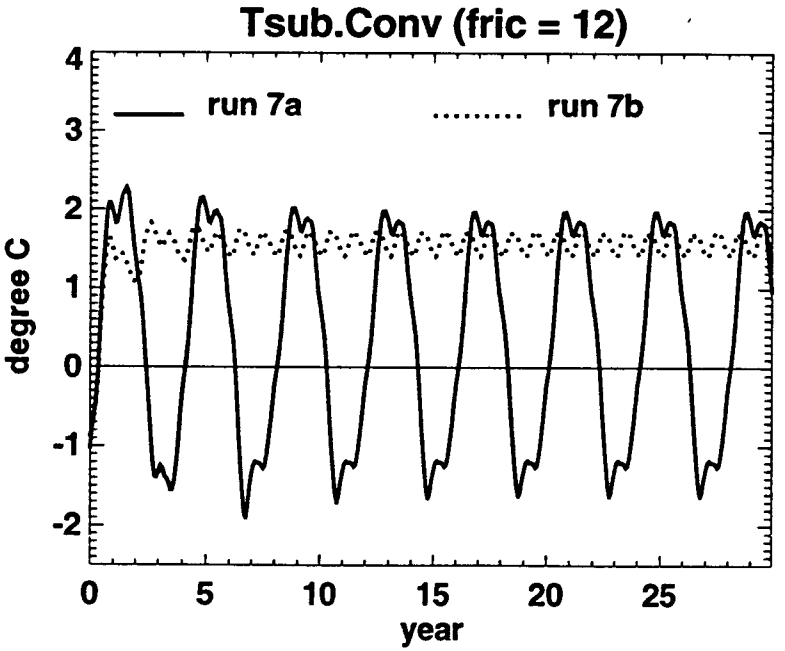
Tsub.Conv (fric = 12)
run 7a
run 7b
degree C
year

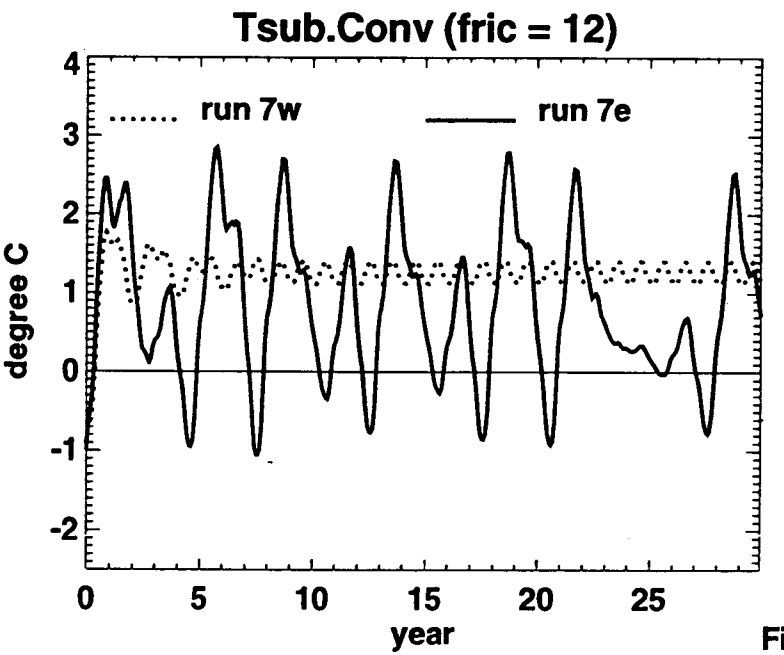
Tsub.Conv (fric = 12)
run 7w
run 7e
degree C
year

Fig.5

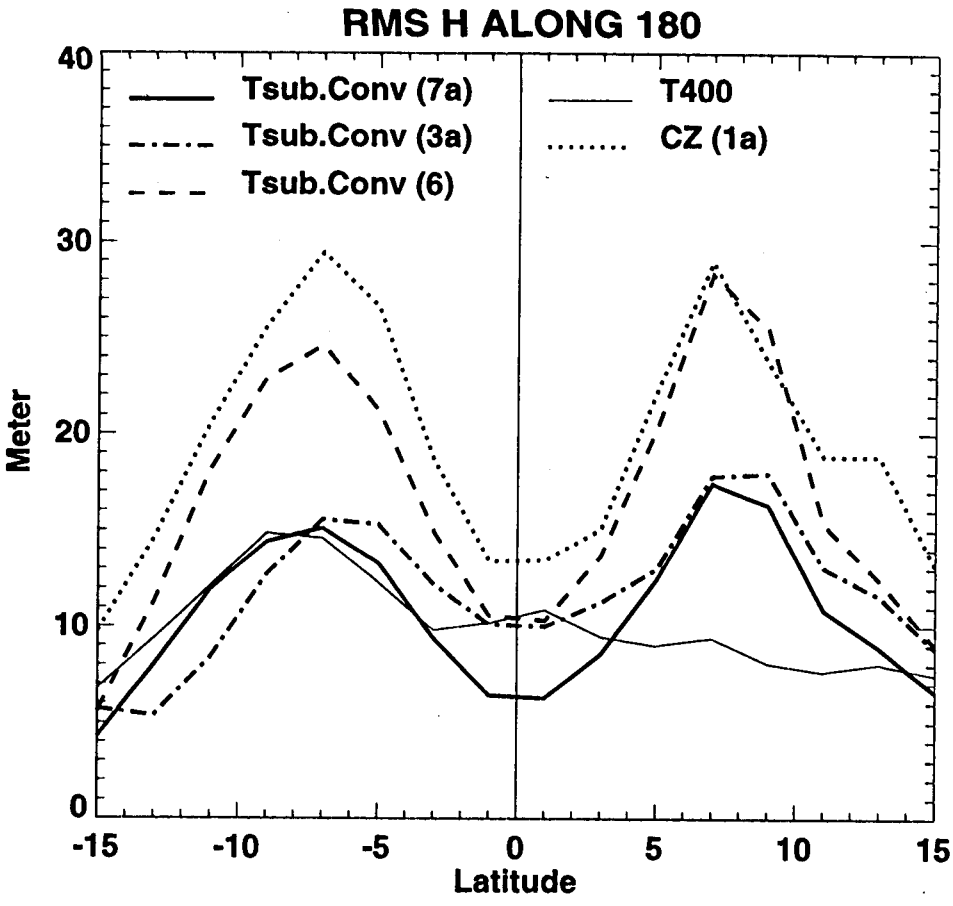
RMS H ALONG 180
Tsub.Conv (7a)
Tsub.Conv (3a)
Tsub.Conv (6)
T400
CZ (1a)
Meter
40
30
20
10
0
-15
-10
-5
0
5
10
15
Latitude

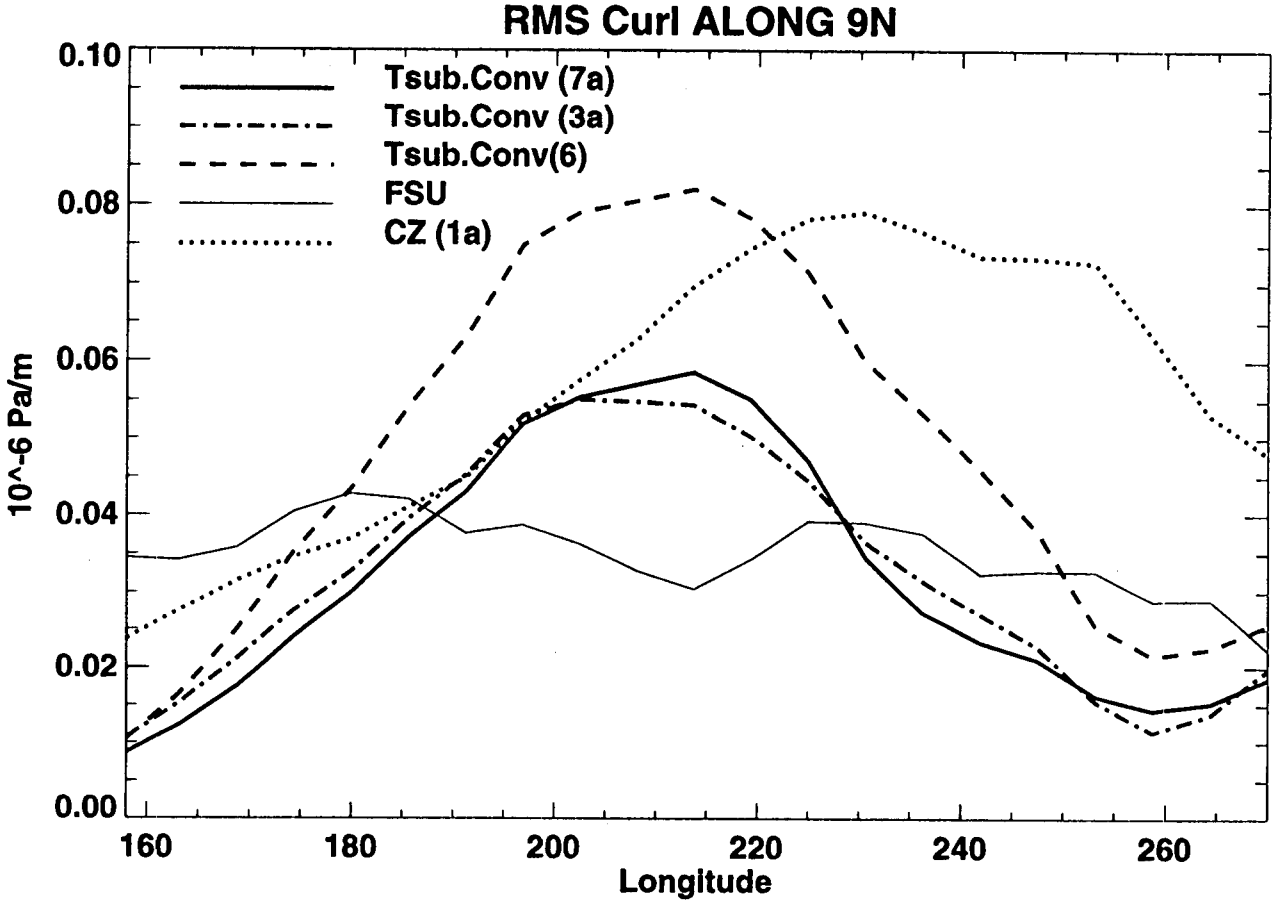
RMS Curl ALONG 9N
Tsub.Conv (7a)
Tsub.Conv (3a)
Tsub.Conv(6)
FSU
CZ (1a)
10^-6 Pa/m
0.10
0.08
0.06
0.04
0.02
0.00
160
180
200
220
240
260
Longitude

Fig.6

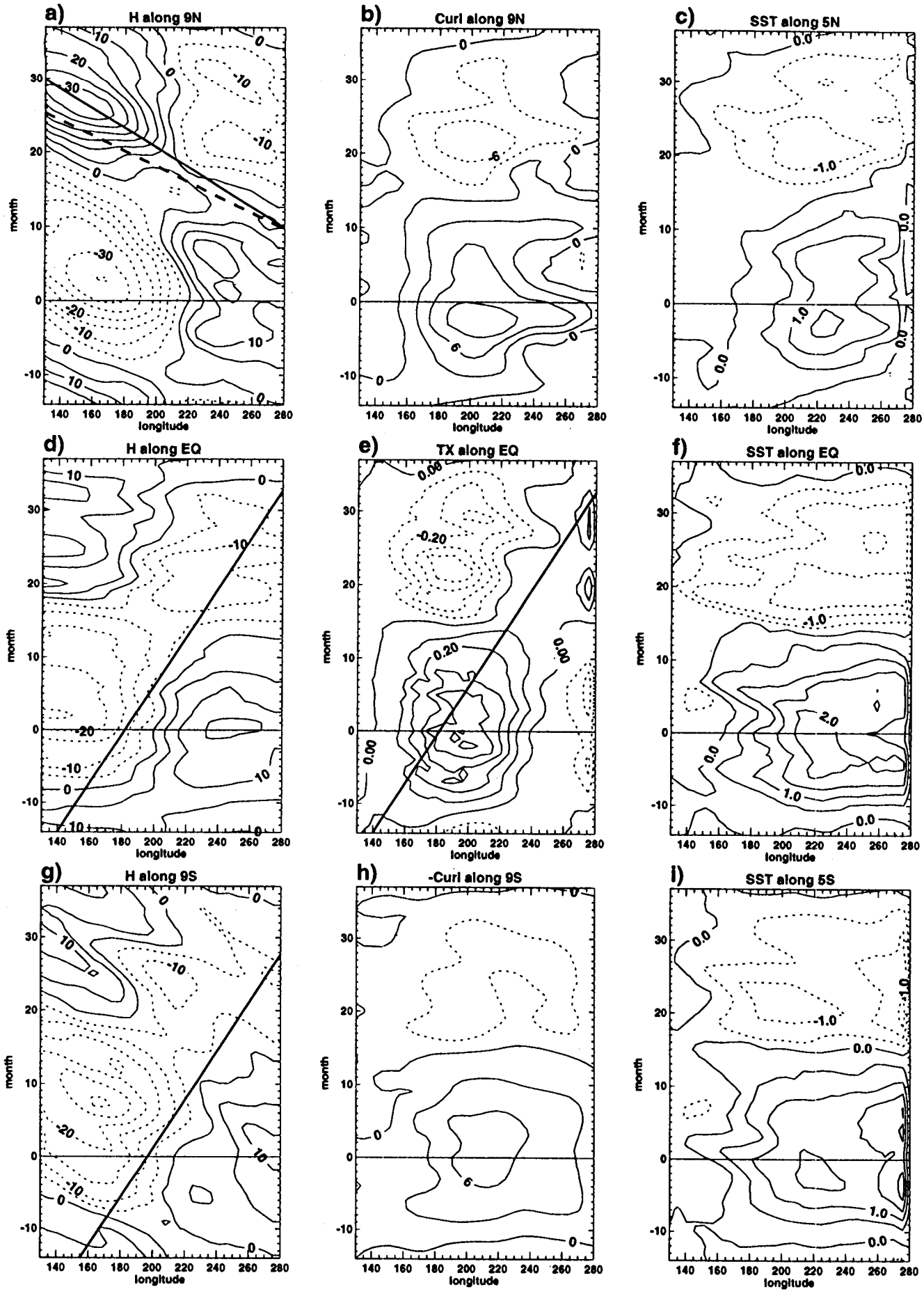
a) H along 9N
b) Curl along 9N
c) SST along 5N
d) H along EQ
e) TX along EQ
f) SST along EQ
g) H along 9S
h) -Curl along 9S
i) SST along 5S
month
longitude

Fig.7

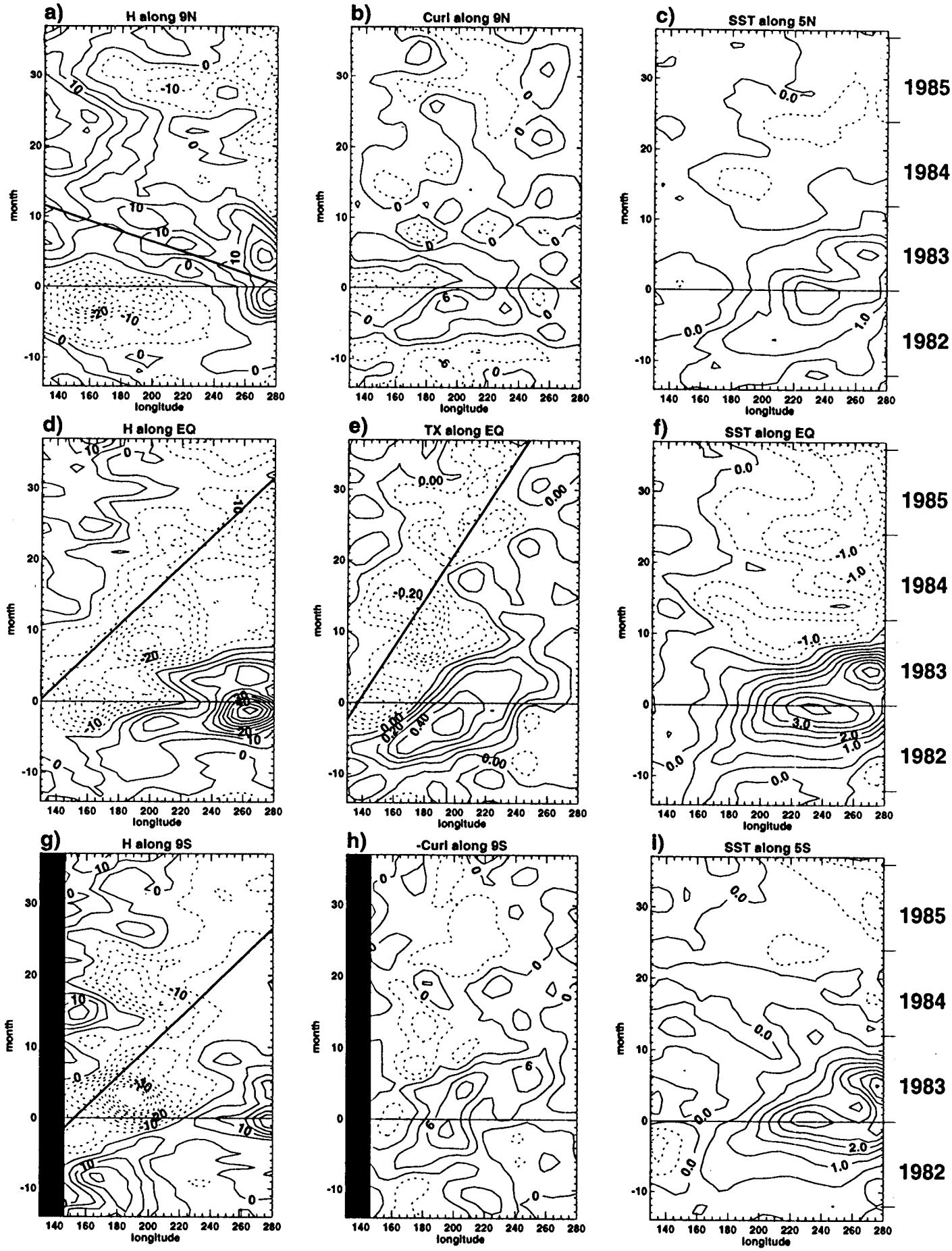
a) H along 9N
b) Curl along 9N
c) SST along 5N
d) H along EQ
e) TX along EQ
f) SST along EQ
g) H along 9S
h) -Curl along 9S
i) SST along 5S
month
longitude
140 160 180 200 220 240 260 280
1985
1984
1983
1982

Fig.8

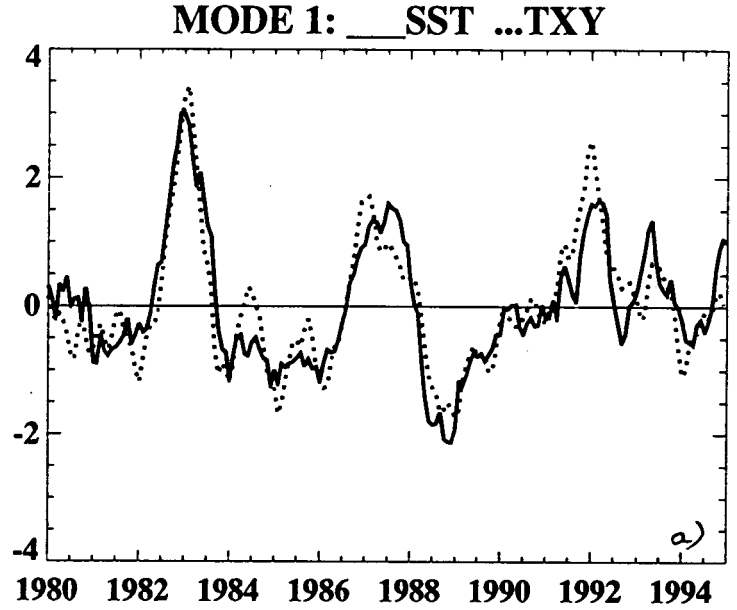
MODE 1: ___SST ...TXY
4
2
0
-2
-4
1980 1982 1984 1986 1988 1990 1992 1994
a)

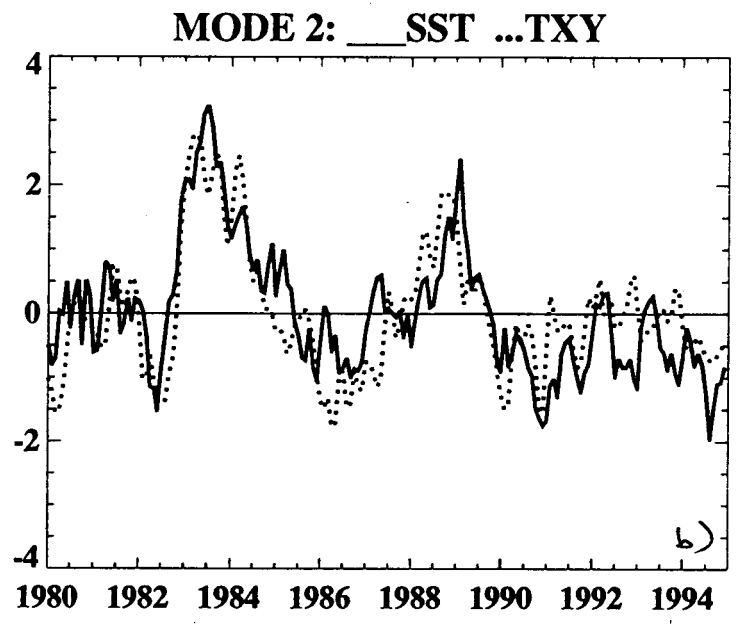
MODE 2: ___SST ...TXY
4
2
0
-2
-4
1980 1982 1984 1986 1988 1990 1992 1994
b)

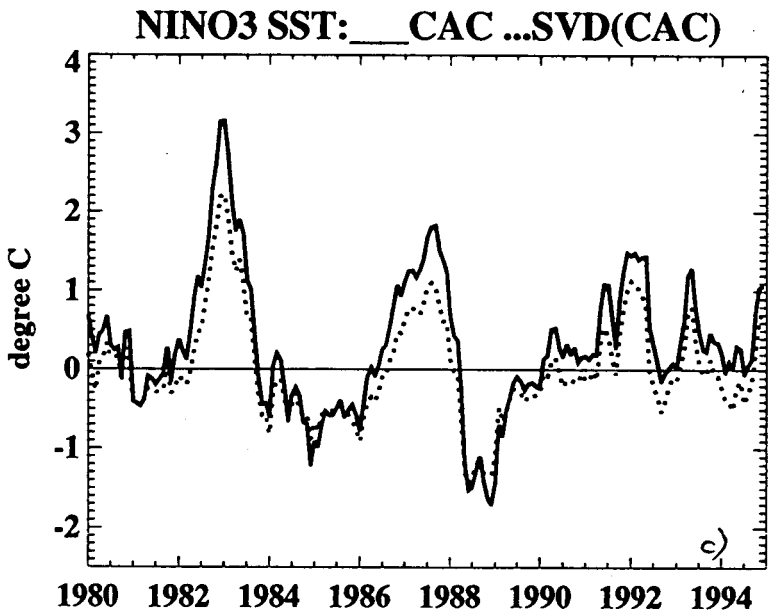
NINO3 SST:___CAC ...SVD(CAC)
degree C
4
3
2
1
0
-1
-2
1980 1982 1984 1986 1988 1990 1992 1994
c)

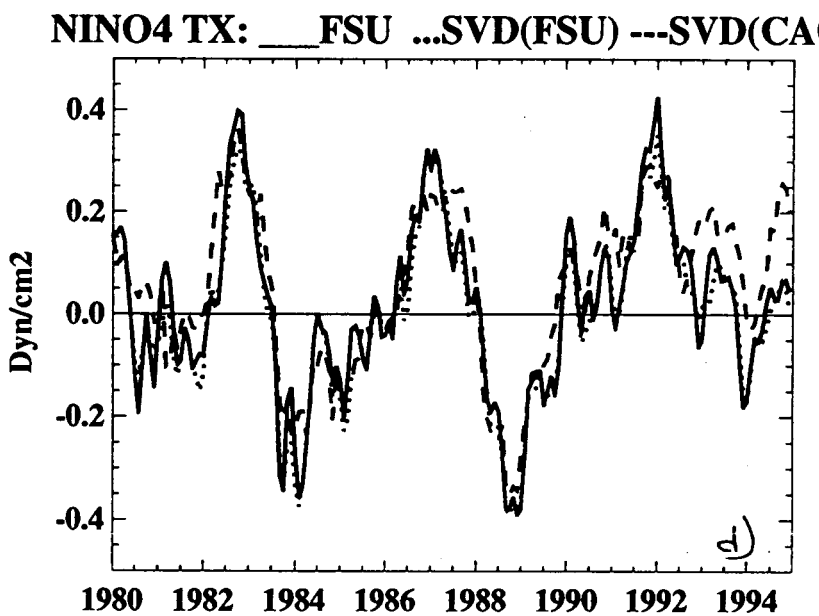
NINO4 TX: ___FSU ...SVD(FSU) ---SVD(CAC)
Dyn/cm2
0.4
0.2
0.0
-0.2
-0.4
1980 1982 1984 1986 1988 1990 1992 1994
d)

Fig.9

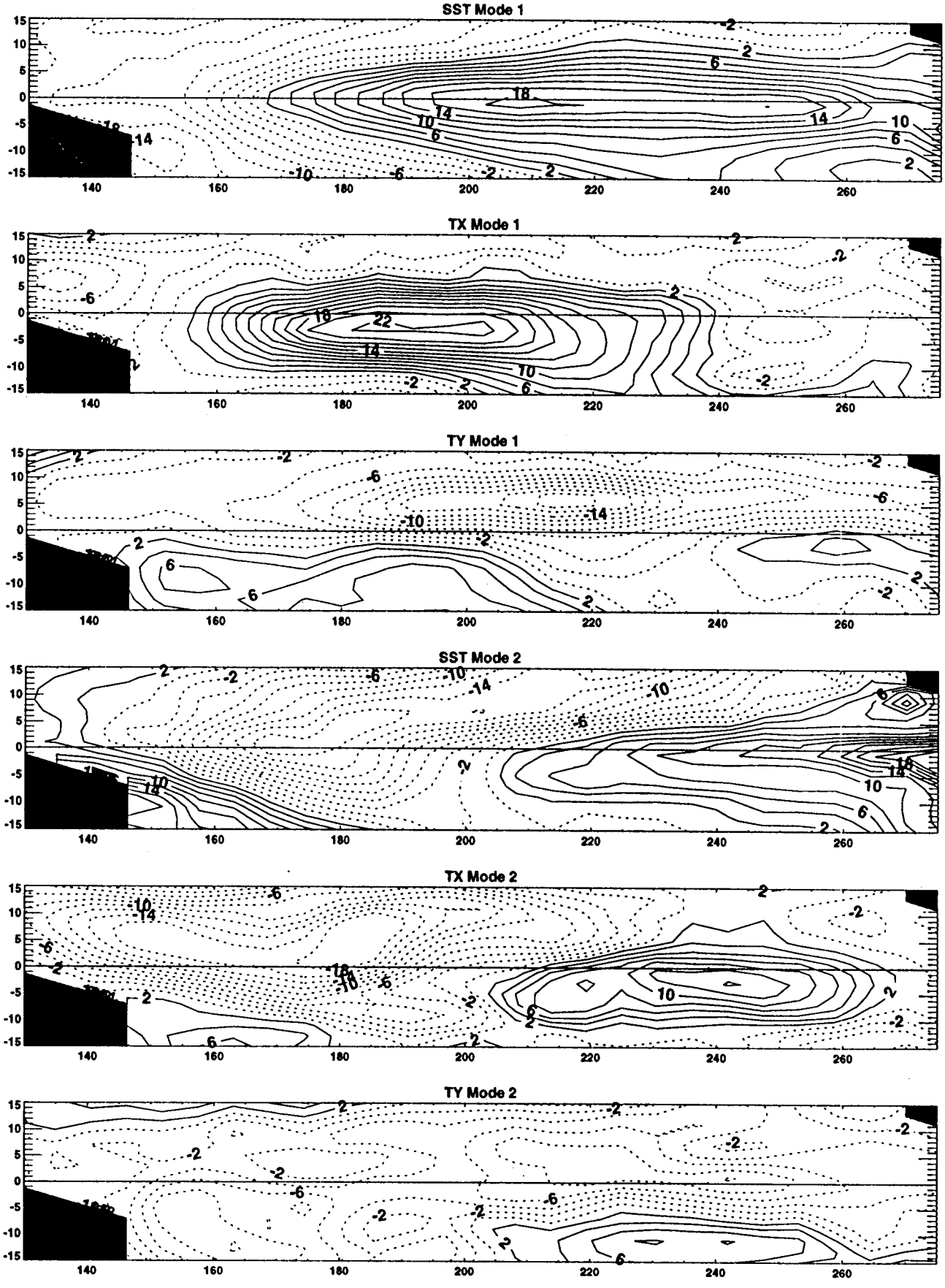
SST Mode 1
TX Mode 1
TY Mode 1
SST Mode 2
TX Mode 2
TY Mode 2
15
10
5
0
-5
-10
-15
140
160
180
200
220
240
260

Fig.10

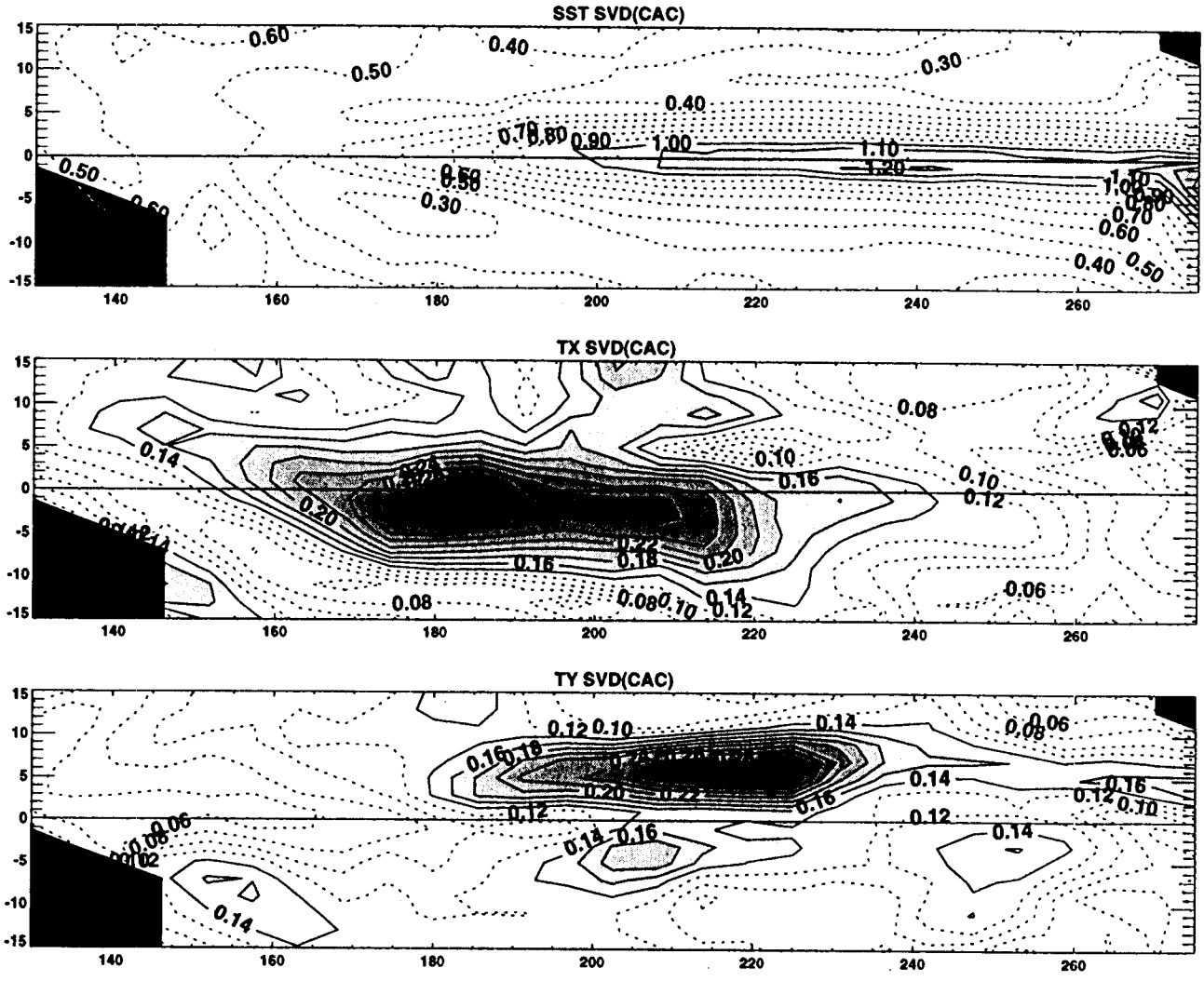

Fig.11

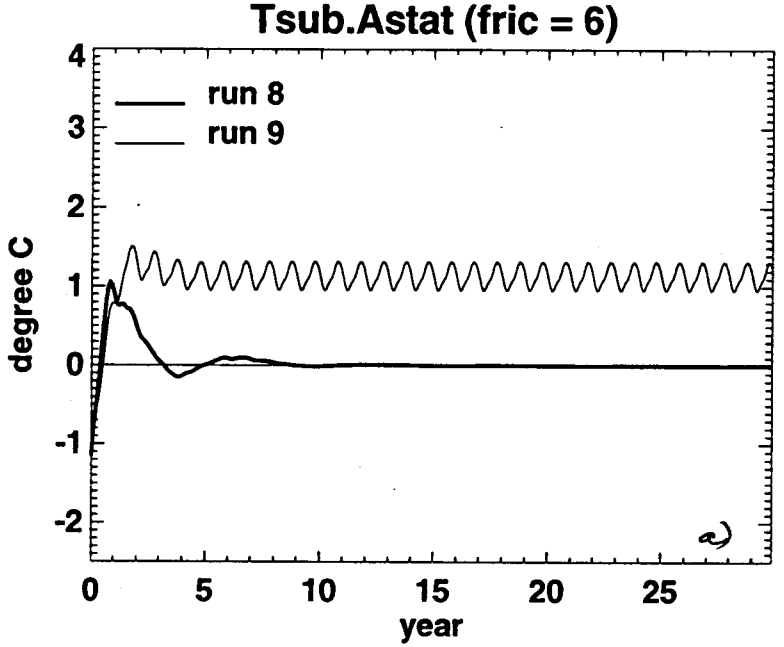
Tsub.Astat (fric = 6)
run 8
run 9
degree C
year
a)

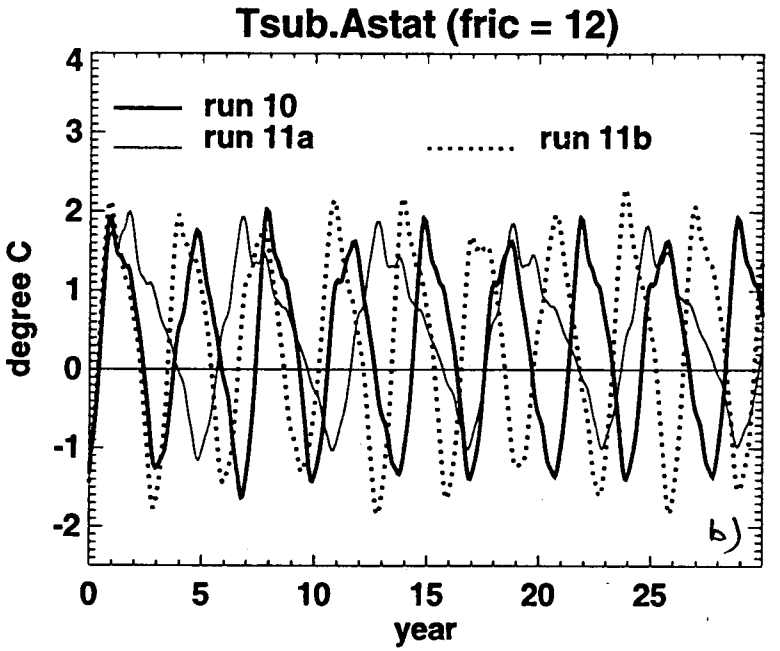
Tsub.Astat (fric = 12)
run 10
run 11a
run 11b
degree C
year
b)

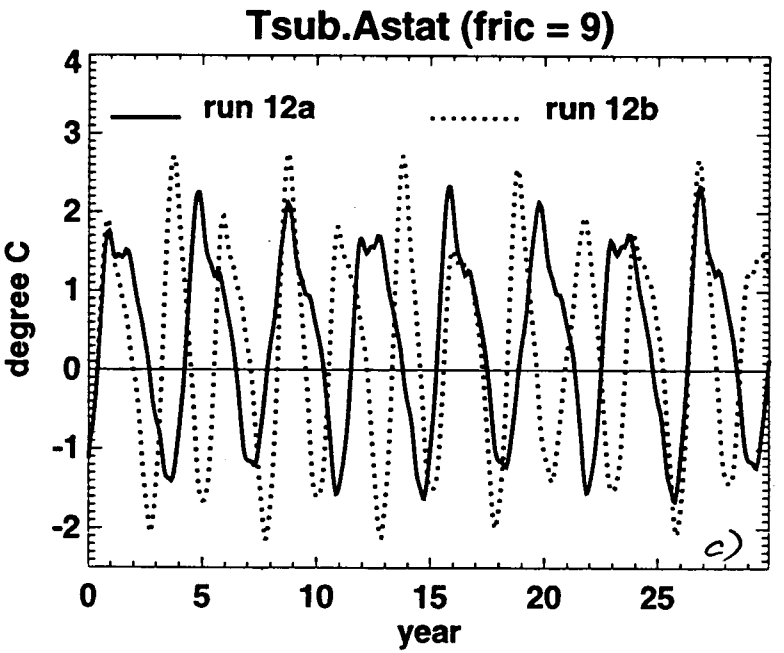
Tsub.Astat (fric = 9)
run 12a
run 12b
degree C
year
c)

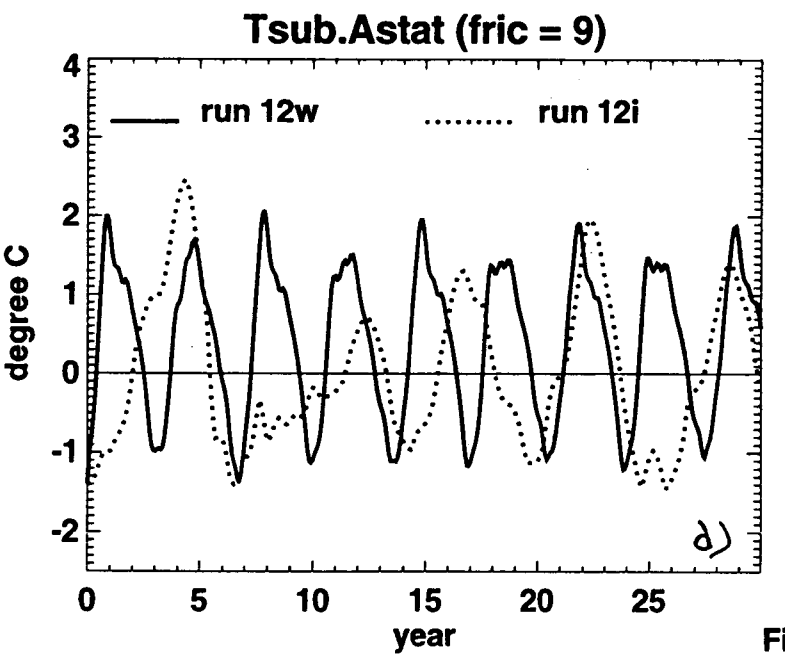
Tsub.Astat (fric = 9)
run 12w
run 12i
degree C
year
d)

Fig.12

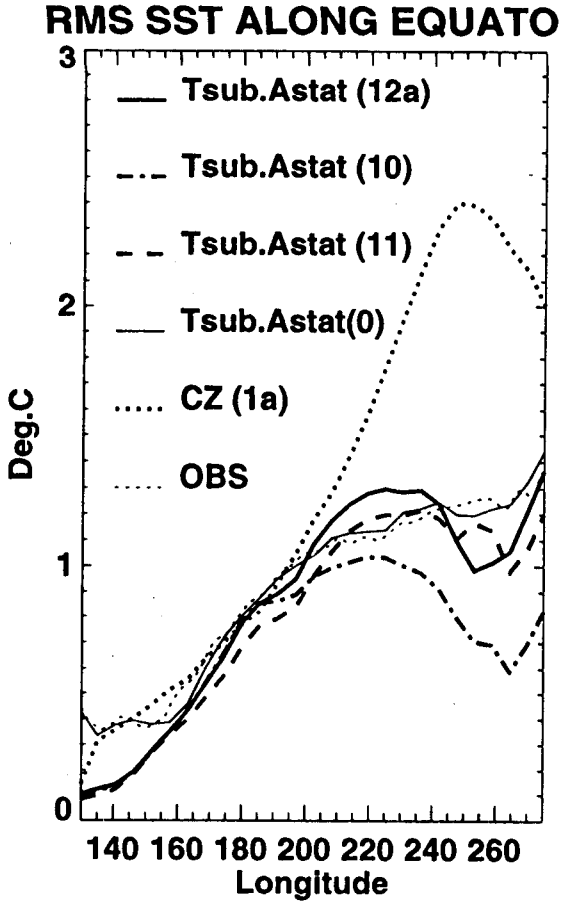
RMS SST ALONG EQUATOR
Tsub.Astat (12a)
Tsub.Astat (10)
Tsub.Astat (11)
Tsub.Astat(0)
CZ (1a)
OBS
Deg.C
0
1
2
3
140 160 180 200 220 240 260
Longitude

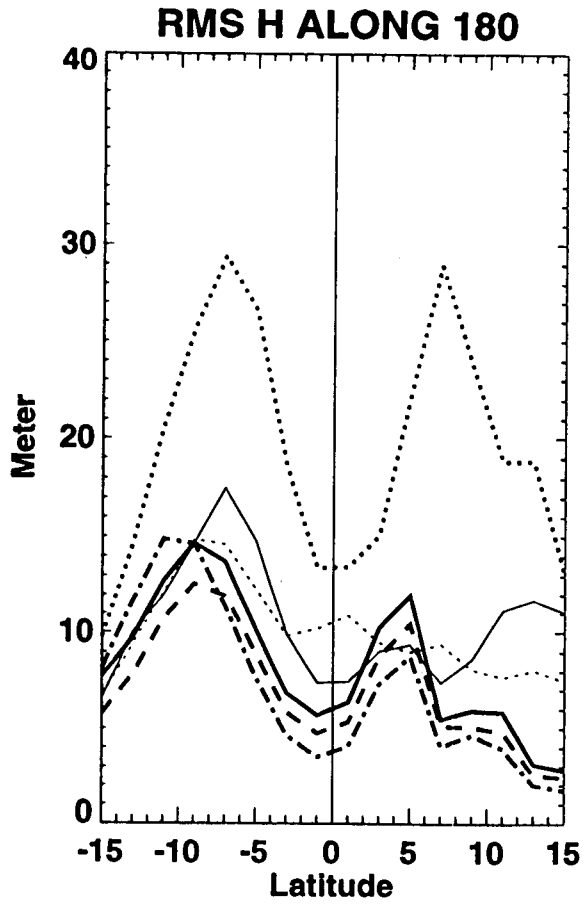
RMS H ALONG 180
Meter
0
10
20
30
40
-15 -10 -5 0 5 10 15
Latitude

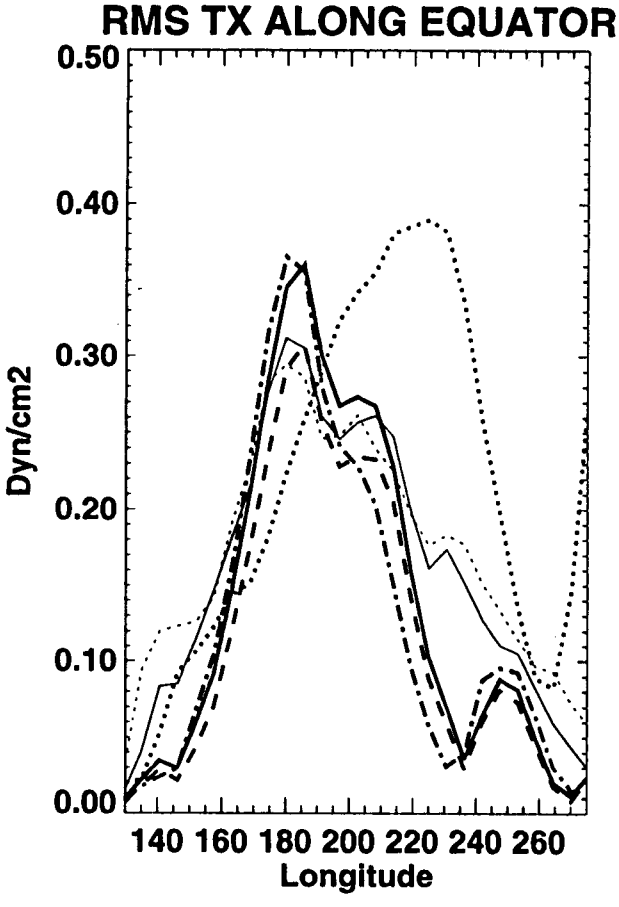
RMS TX ALONG EQUATOR
Dyn/cm2
0.00
0.10
0.20
0.30
0.40
0.50
140 160 180 200 220 240 260
Longitude

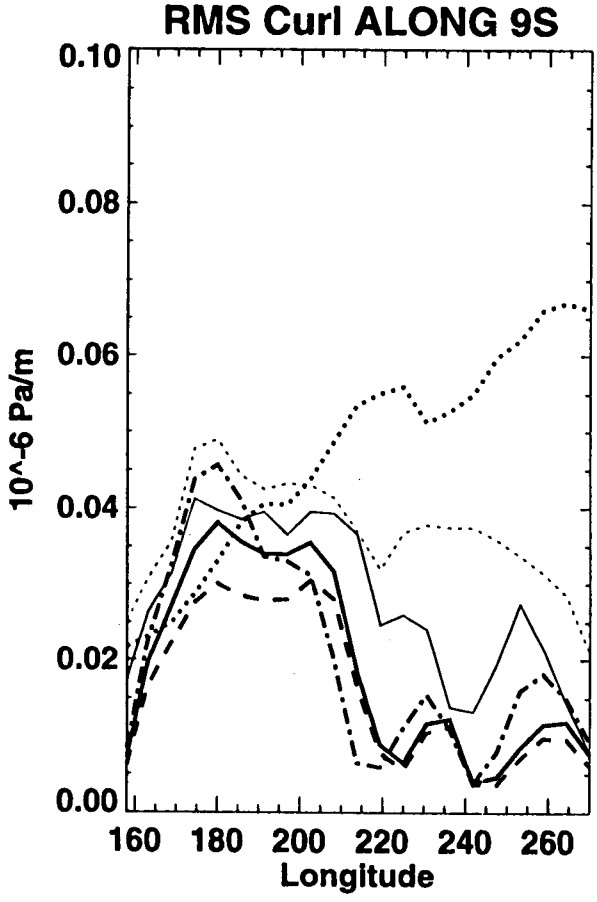
RMS Curl ALONG 9S
10^-6 Pa/m
0.00
0.02
0.04
0.06
0.08
0.10
160 180 200 220 240 260
Longitude

Fig. 13

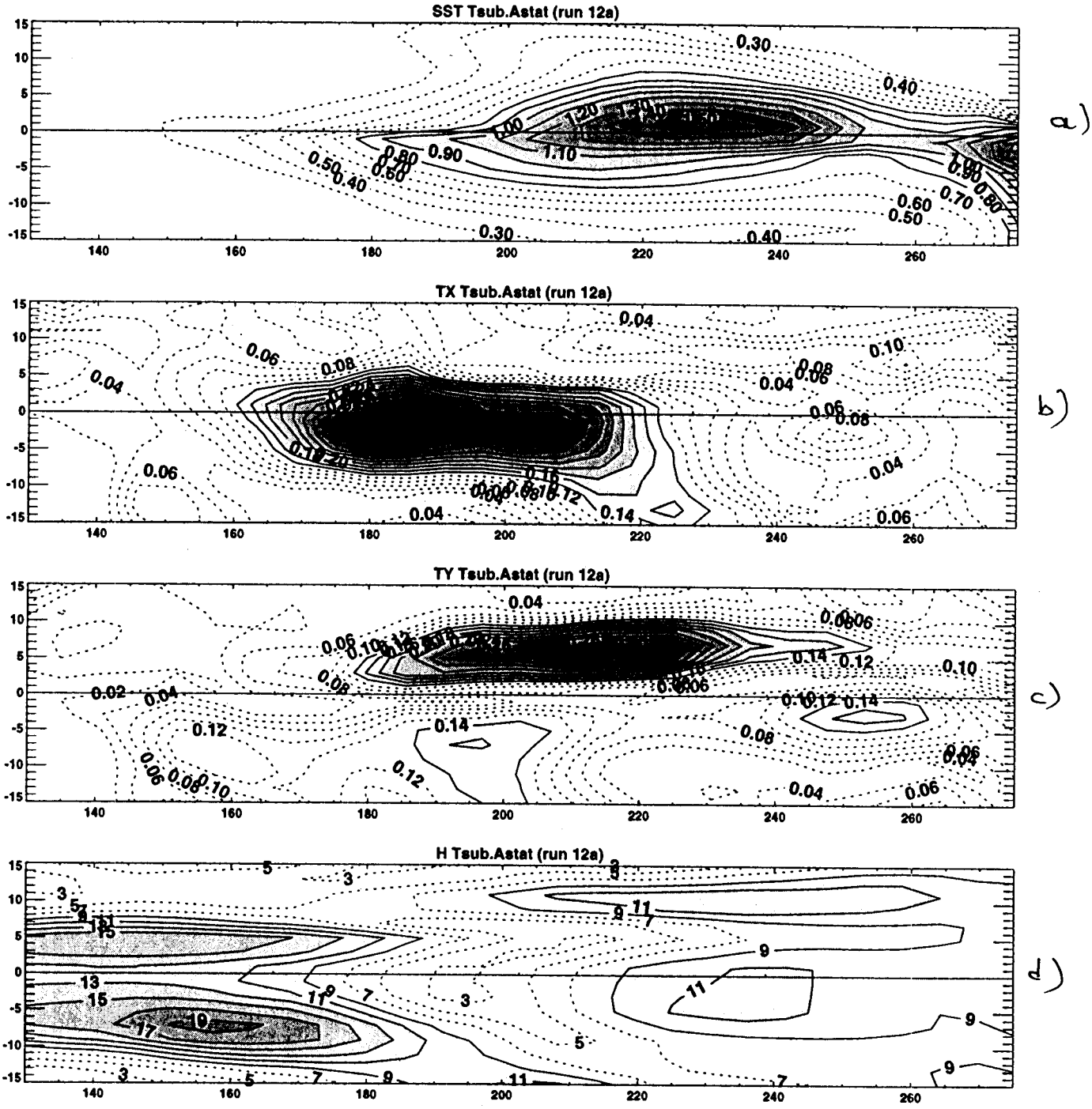
SST Tsub.Astat (run 12a)
a)
TX Tsub.Astat (run 12a)
b)
TY Tsub.Astat (run 12a)
c)
H Tsub.Astat (run 12a)
d)

Fig.14

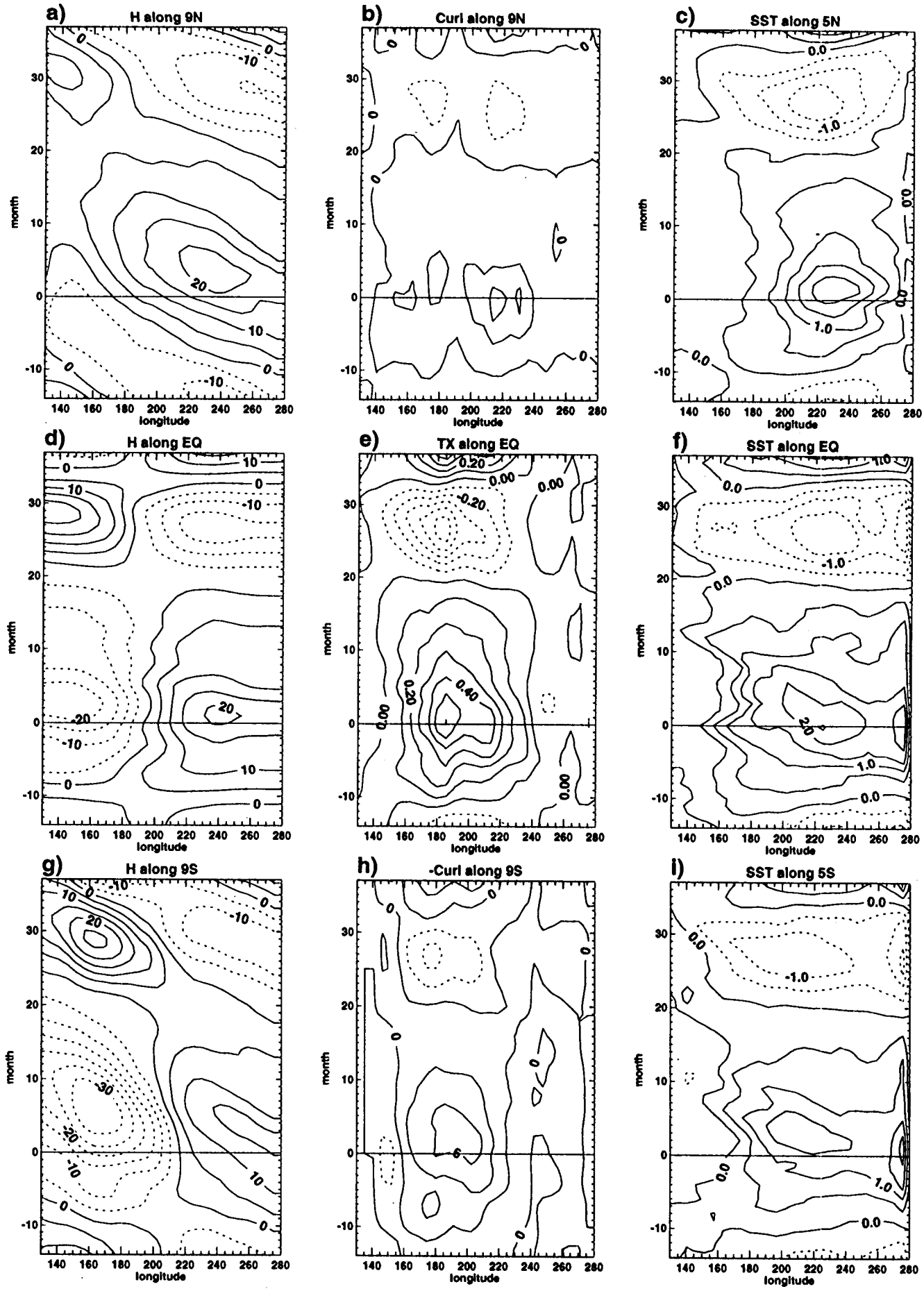
a)
H along 9N
b)
Curl along 9N
c)
SST along 5N
d)
H along EQ
e)
TX along EQ
f)
SST along EQ
g)
H along 9S
h)
-Curl along 9S
i)
SST along 5S
month
longitude

Fig.15

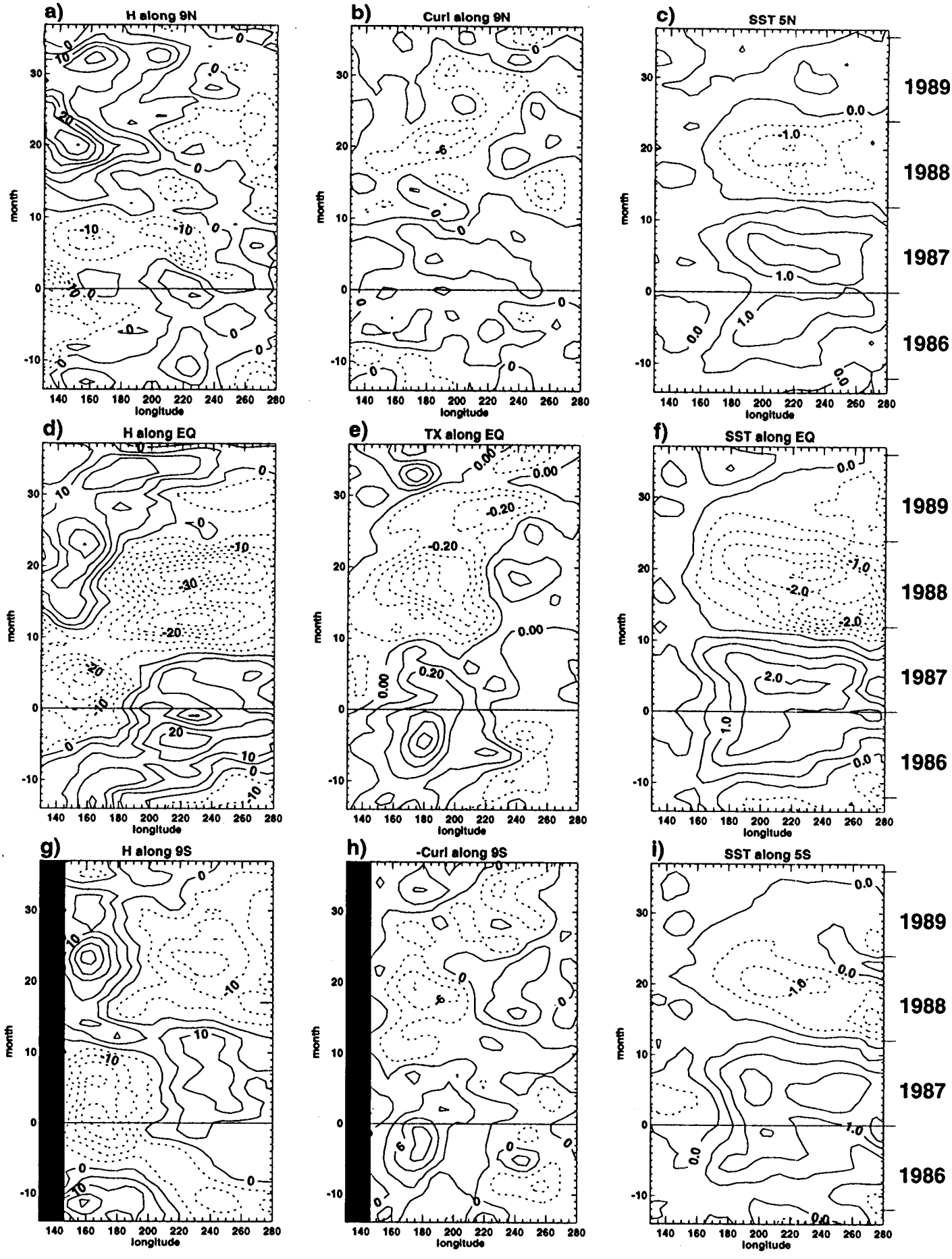
a) H along 9N
b) Curl along 9N
c) SST 5N
d) H along EQ
e) TX along EQ
f) SST along EQ
g) H along 9S
h) -Curl along 9S
i) SST along 5S
month
longitude
1989
1988
1987
1986

Fig.16

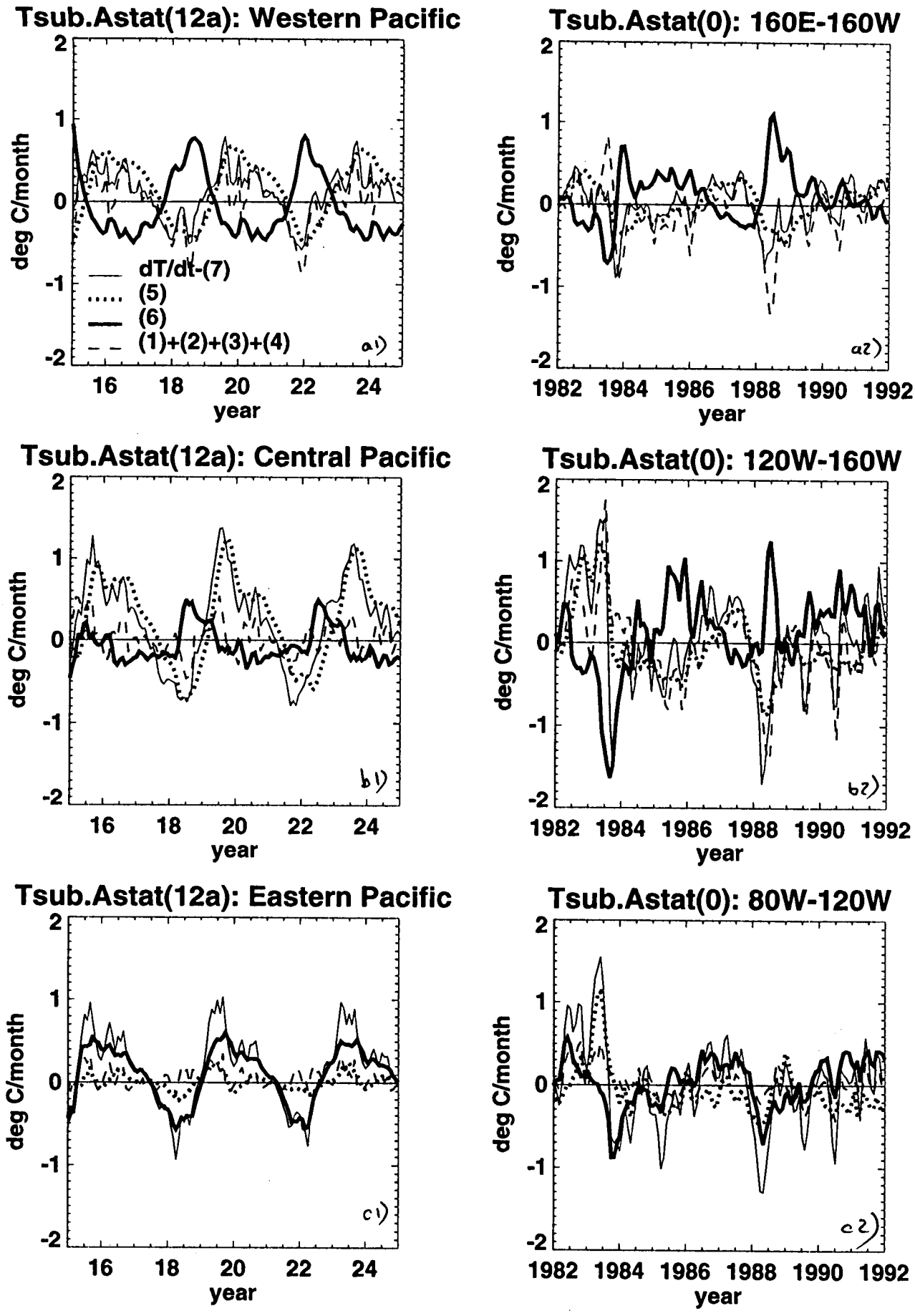
Tsub.Astat(12a): Western Pacific
Tsub.Astat(0): 160E-160W
Tsub.Astat(12a): Central Pacific
Tsub.Astat(0): 120W-160W
Tsub.Astat(12a): Eastern Pacific
Tsub.Astat(0): 80W-120W
deg C/month
year
dT/dt-(7)
(5)
(6)
(1)+(2)+(3)+(4)
a1)
a2)
b1)
b2)
c1)
c2)

Fig.17

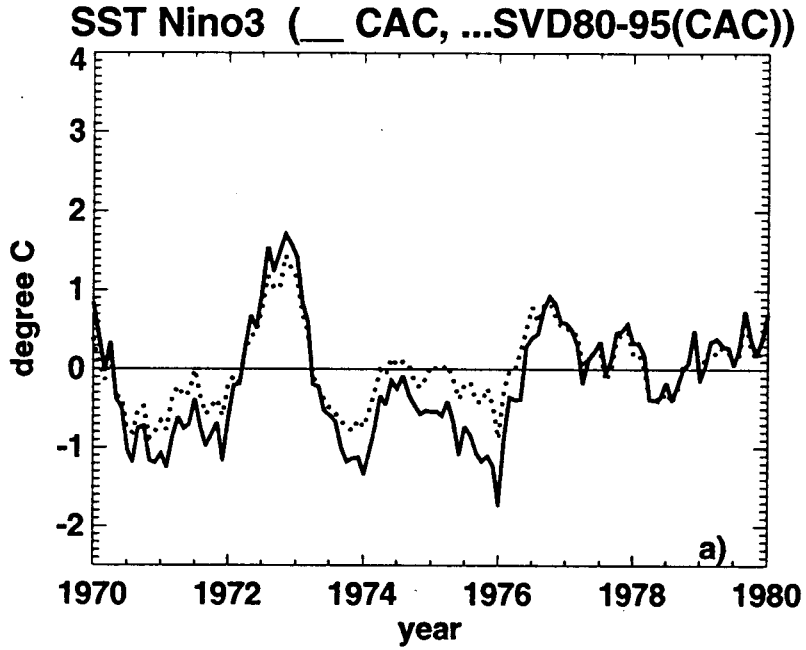
SST Nino3 (__ CAC, ...SVD80-95(CAC))
degree C
4
3
2
1
0
-1
-2
a)
1970
1972
1974
1976
1978
1980
year

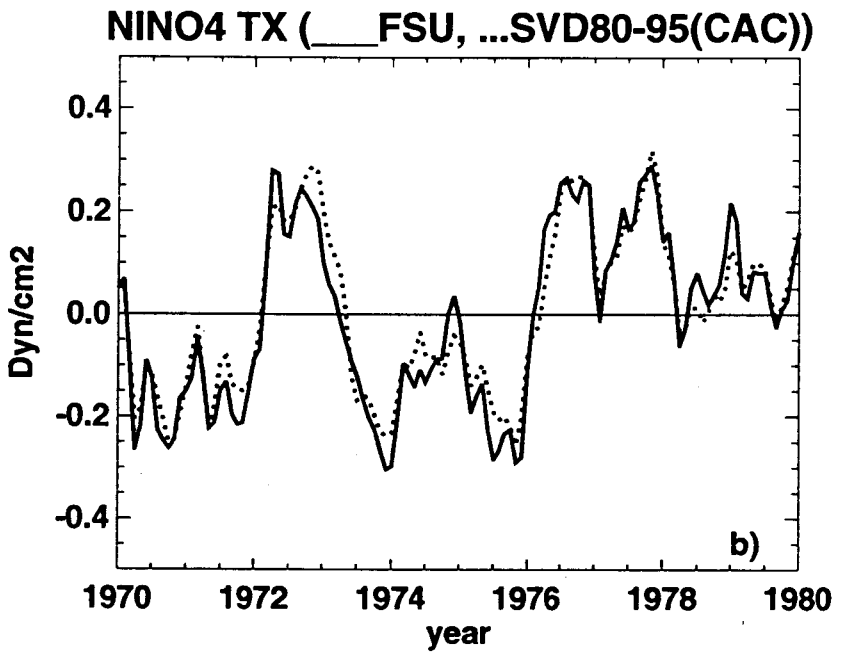
NINO4 TX (___FSU, ...SVD80-95(CAC))
Dyn/cm2
0.4
0.2
0.0
-0.2
-0.4
b)
1970
1972
1974
1976
1978
1980
year

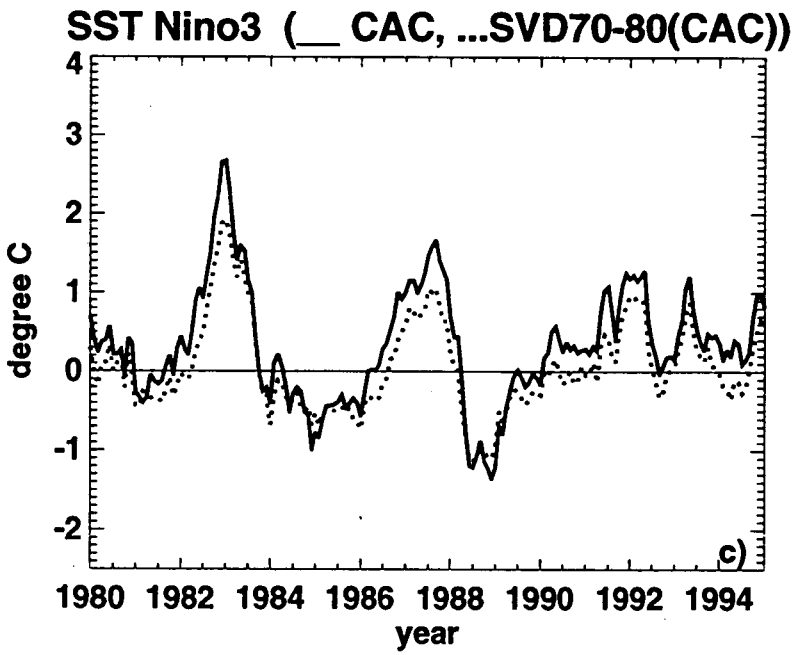
SST Nino3 (__ CAC, ...SVD70-80(CAC))
degree C
4
3
2
1
0
-1
-2
c)
1980
1982
1984
1986
1988
1990
1992
1994
year

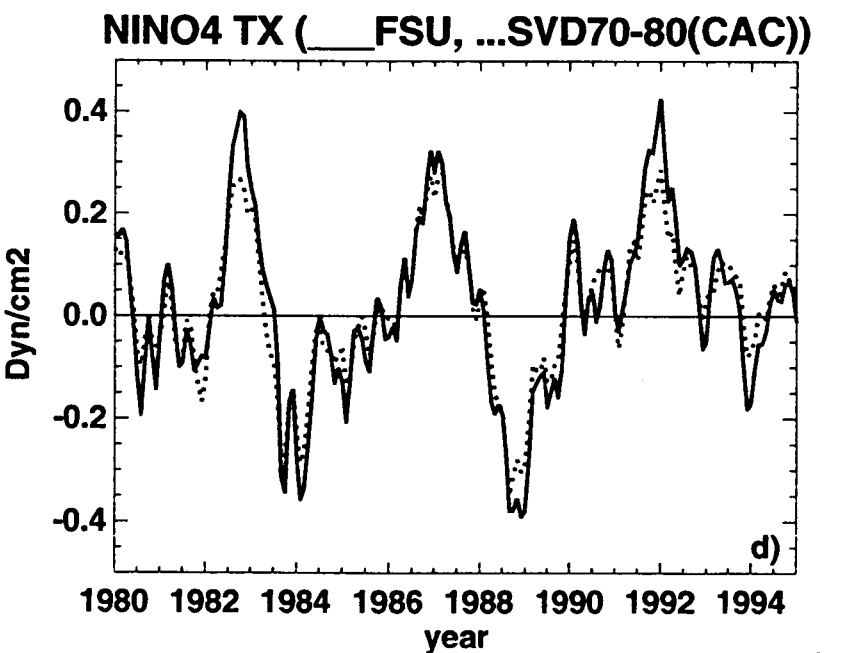
NINO4 TX (___FSU, ...SVD70-80(CAC))
Dyn/cm2
0.4
0.2
0.0
-0.2
-0.4
d)
1980
1982
1984
1986
1988
1990
1992
1994
year

Fig.18

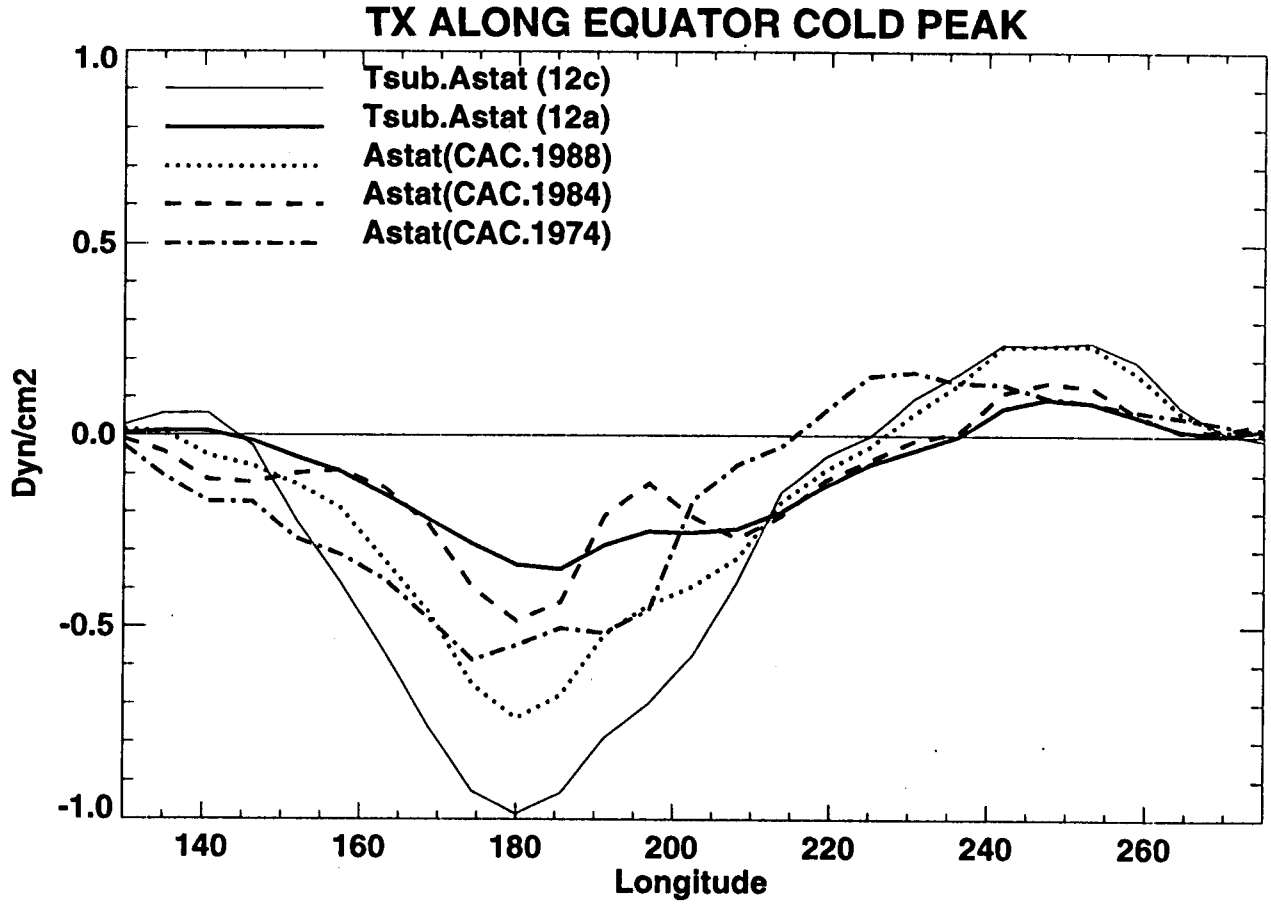
TX ALONG EQUATOR COLD PEAK
Tsub.Astat (12c)
Tsub.Astat (12a)
Astat(CAC.1988)
Astat(CAC.1984)
Astat(CAC.1974)
1.0
0.5
0.0
-0.5
-1.0
Dyn/cm2
140
160
180
200
220
240
260
Longitude

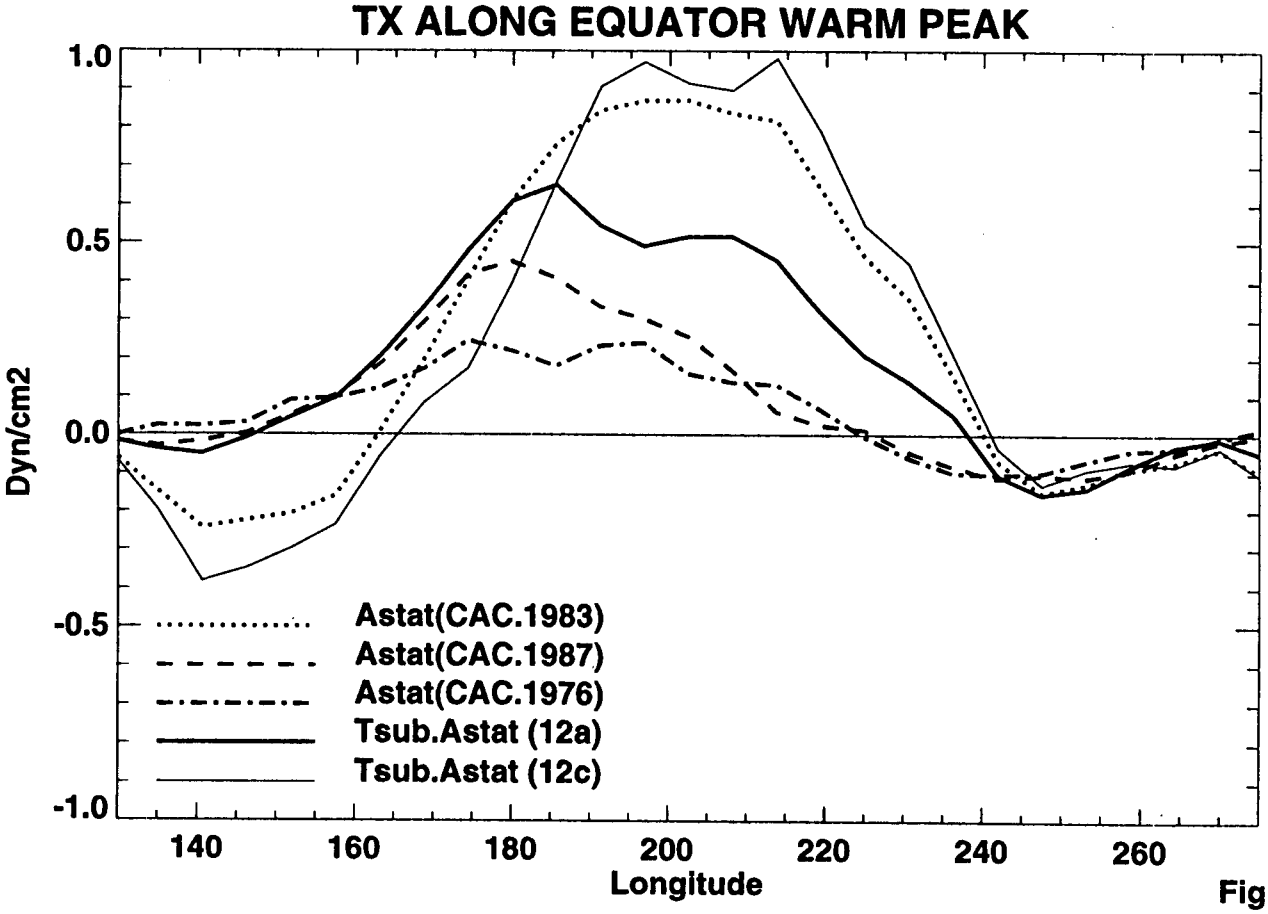
TX ALONG EQUATOR WARM PEAK
Astat(CAC.1983)
Astat(CAC.1987)
Astat(CAC.1976)
Tsub.Astat (12a)
Tsub.Astat (12c)
1.0
0.5
0.0
-0.5
-1.0
Dyn/cm2
140
160
180
200
220
240
260
Longitude

Fig.19

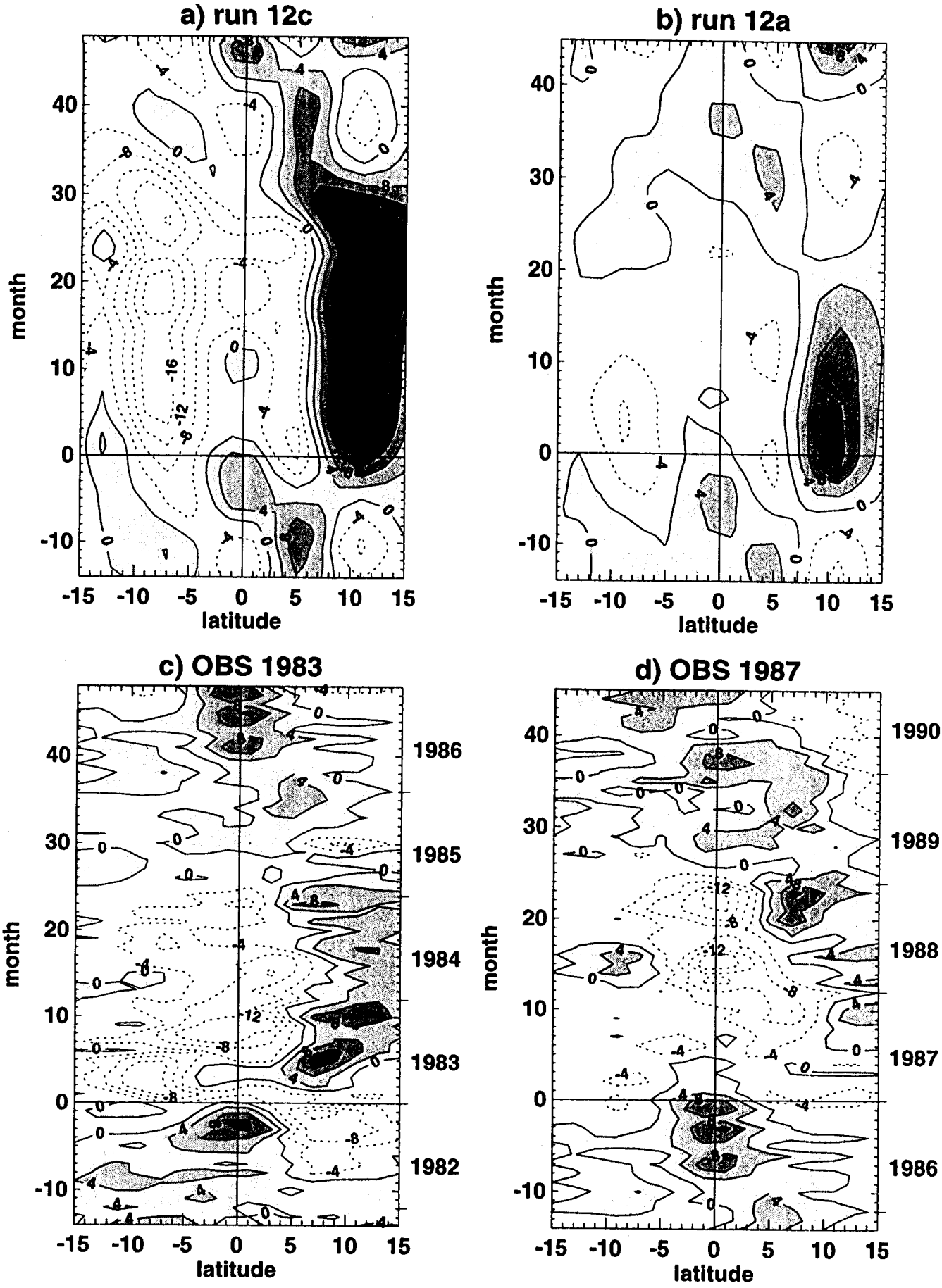
a) run 12c
b) run 12a
c) OBS 1983
d) OBS 1987
month
latitude
1986
1985
1984
1983
1982
1990
1989
1988
1987
1986

Fig.20

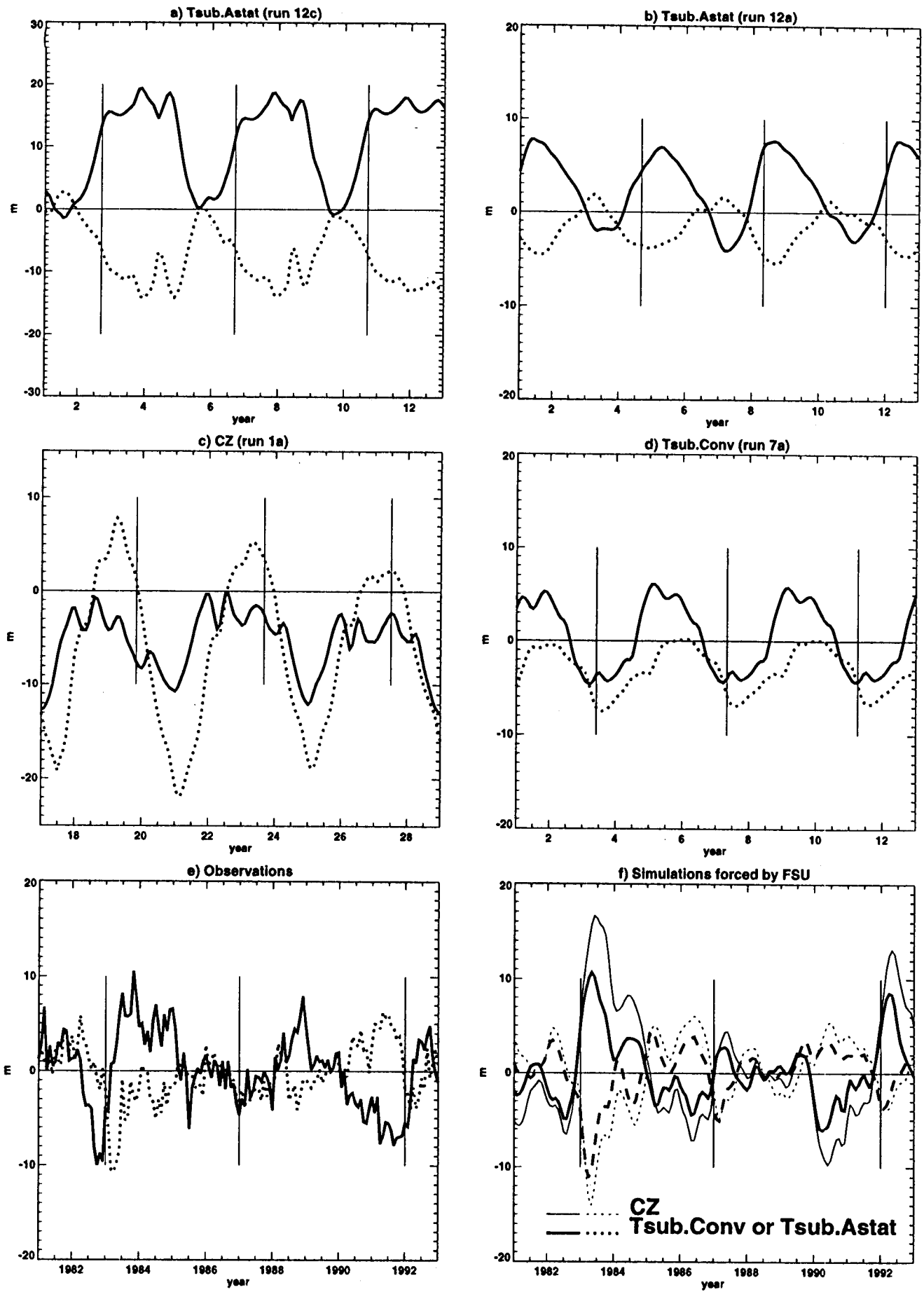
a) Tsub.Astat (run 12c)
b) Tsub.Astat (run 12a)
c) CZ (run 1a)
d) Tsub.Conv (run 7a)
e) Observations
f) Simulations forced by FSU
E
year
CZ
Tsub.Conv or Tsub.Astat

Fig.21

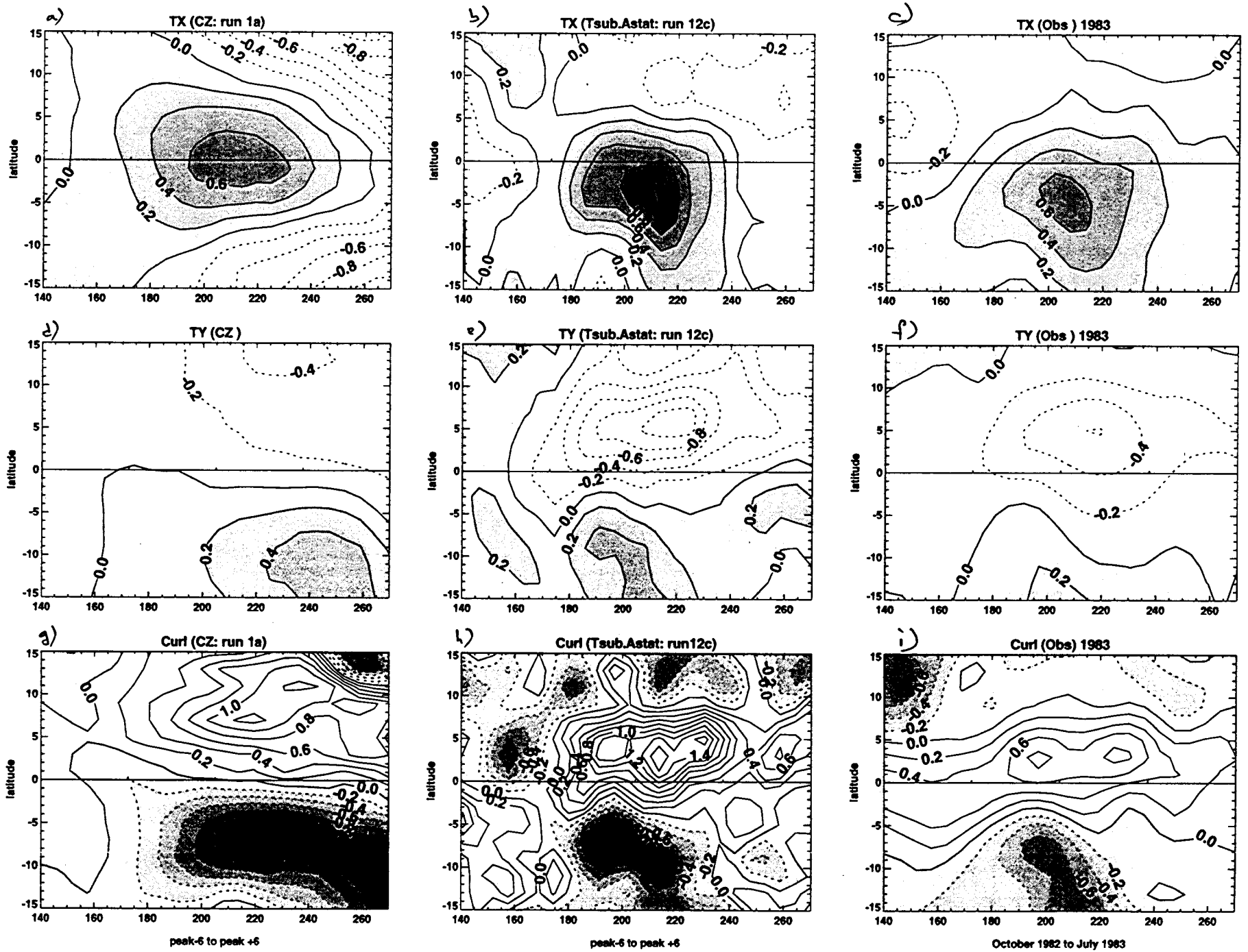
a)
TX (CZ: run 1a)
b)
TX (Tsub.Astat: run 12c)
c)
TX (Obs) 1983
d)
TY (CZ)
e)
TY (Tsub.Astat: run 12c)
f)
TY (Obs) 1983
g)
Curl (CZ: run 1a)
h)
Curl (Tsub.Astat: run12c)
i)
Curl (Obs) 1983
latitude
peak-6 to peak +6
peak-6 to peak +6
October 1982 to July 1983

Fig.22

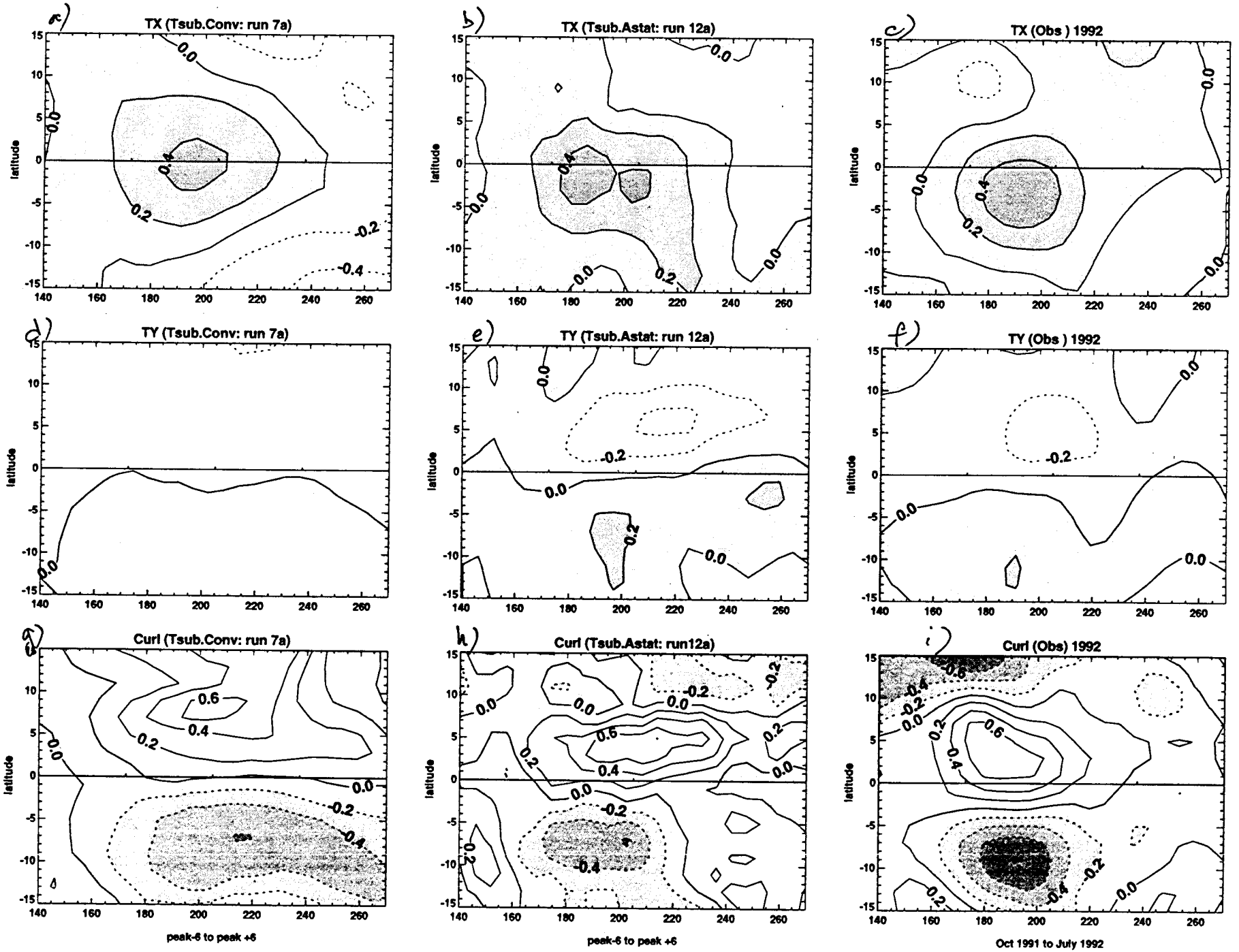
a)
TX (Tsub.Conv: run 7a)
b)
TX (Tsub.Astat: run 12a)
c)
TX (Obs) 1992
d)
TY (Tsub.Conv: run 7a)
e)
TY (Tsub.Astat: run 12a)
f)
TY (Obs) 1992
g)
Curl (Tsub.Conv: run 7a)
h)
Curl (Tsub.Astat: run12a)
i)
Curl (Obs) 1992
latitude
peak-6 to peak +6
peak-6 to peak +6
Oct 1991 to July 1992

Fig.23

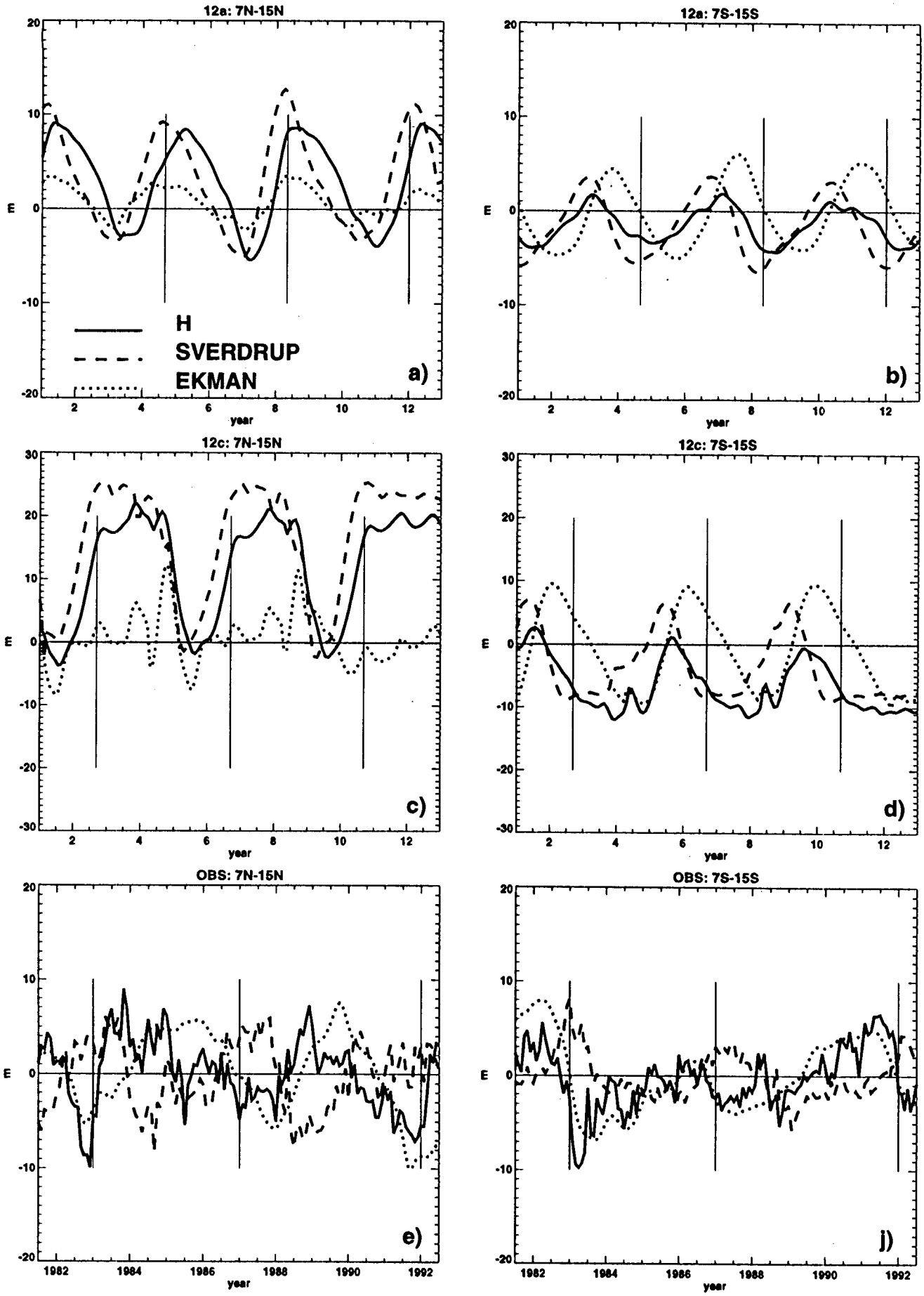
12a: 7N-15N
12a: 7S-15S
12c: 7N-15N
12c: 7S-15S
OBS: 7N-15N
OBS: 7S-15S
H
SVERDRUP
EKMAN
a)
b)
c)
d)
e)
j)
E
year

Fig.24